# XBeach skillbed report, revision 4509

**status update trunk_default**

Revision: 4509

April 17, 2015

**XBeach skillbed report, revision 4509**

Published and printed by:

Deltares
Rotterdamseweg 185
p.o. box 177
2600 MH Delft
The Netherlands

telephone: +31 88 335 85 85
fax: +31 88 335 85 82
e-mail: info@deltares.nl
www: http://www.deltares.nl

For support contact:

telephone: +31 88 335 85 55
fax: +31 88 335 81 11
e-mail: xbeach@deltares.nl
www: http://www.xbeach.org/

Copyright © 2015 Deltares
All rights reserved. No part of this document may be reproduced in any form by print, photo print, photo copy, microfilm or any other means, without written permission from the publisher: Deltares.

# Contents

# Chapter 1

# Introduction

## 1.1 Introduction to the XBeach model

The devastating effects of hurricanes on low-lying sandy coasts, especially during the 2004 and 2005 seasons have pointed at an urgent need to be able to assess the vulnerability of coastal areas and (re-)design coastal protection for future events, and also to evaluate the performance of existing coastal protection projects compared to 'do-nothing' scenarios. In view of this the Morphos-3D project was initiated by USACE-ERDC, bringing together models, modelers and data on hurricane winds, storm surges, wave generation and nearshore processes. As part of this initiative an open-source program, XBeach for eXtreme Beach behaviour, has been developed to model the nearshore response to hurricane impacts. The model includes wave breaking, surf and swash zone processes, dune erosion, overwashing and breaching (Roelvink et al., 2009).

Existing tools to assess dune erosion under extreme storm conditions assume alongshore uniform conditions and have been applied successfully along relatively undisturbed coasts (Vellinga, 1986; Steetzel, 1993; Nishi and Kraus, 1996; Larson et al., 2004), but are inadequate to assess the more complex situation where the coast has significant alongshore variability. This variability may result from anthropogenic causes, such as the presence of artificial inlets, sea walls, and revetments, but also from natural causes, such as the variation in dune height along the coast or the presence of rip channels and shoals on the shoreface (Thornton et al., 2007). A particularly complex situation is found when barrier islands protect storm impact on the main land coast. In that case the elevation, width and length of the barrier island, as well as the hydrodynamic conditions (surge level) of the back bay should be taken into account to assess the coastal response. Therefore, the assessment of storm impact in these more complex situations requires a two-dimensional process-based prediction tool, which contains the essential physics of dune erosion and overwash, avalanching, swash motions, infragravity waves and wave groups.

With regard to dune erosion, the development of a scarp andepisodic slumping after undercutting is a dominant process (Van Gent et al., 2008). This supplies sand to the swash and surf zone that is transported seaward by the backwash motion and by the undertow; without it the upper beach scours down and the dune erosion process slows down considerably. One-dimensional (cross-shore) models such as DUROSTA (Steetzel, 1993) focus on the underwater offshore transport and obtain the supply of sand by extrapolating these transports to the dry dune. Overton and Fisher (1988), Nishi and Kraus (1996) focus on the supply of sand by the dune based on the concept of wave impact. Both approaches rely on heuristic estimates of

the runup and are well suited for 1D application but difficult to apply in a horizontally 2D setting. Hence, a more comprehensive modelling of the swash motions is called for.

Swash motions are up to a large degree a result from wave-group forcing of infragravity waves (Tucker, 1954). Depending on the beach configuration and directional properties of the incident wave spectrum both leaky and trapped infragravity waves contribute to the swash spectrum (Huntley et al., 1981). Raubenheimer and Guza (1996) show that incident band swash is saturated, infragravity swash is not, therefore infragravity swash is dominant in storm conditions. Models range from empirical formulations (e.g. Stockdon et al., 2006) through analytical approaches (Schaeffer, 1994; Erikson et al., 2005) to numerical models in 1D (e.g. List, 1992; Roelvink, 1993b) and 2DH (e.g. Van Dongeren et al., 2003; Reniers et al., 2004a, 2006). 2DH wavegroup resolving models are well capable of describing low-frequency motions. However, for such a model to be applied for swash, a robust drying/flooding formulation is required.

## 1.2 Model approach and innovations

Our aim is to model processes in different regimes as described by Sallenger (2000). He defines an Impact Level to denote different regimes of impact on barrier islands by hurricanes, which are the 1) swash regime, 2) collision regime, 3) overwash regime and 4) inundation regime. The approach we follow to model the processes in these regimes is described below.

To resolve the swash dynamics the model employs a novel 2DH description of the wave groups and accompanying infragravity waves over an arbitrary bathymetry (thus including bound, free and refractively trapped infragravity waves). The wave-group forcing is derived from the time-varying wave-action balance (e.g. Phillips, 1977) with a dissipation model for use in combination with wave groups (Roelvink, 1993a). A roller model (Svendsen, 1984; Nairn et al., 1990; Stive and De Vriend, 1994) is used to represent momentum stored in surface rollers which leads to a shoreward shift in wave forcing.

The wave-group forcing drives infragravity motions and both longshore and cross-shore currents. Wave-current interaction within the wave boundary layer results in an increased wave-averaged bed shear stress acting on the infragravity waves and currents (e.g. Soulsby et al., 1993, and references therein). To account for the randomness of the incident waves the description by Feddersen et al. (2000) is applied which showed good skill for longshore current predictions using a constant drag coefficient (Ruessink et al., 2001).

During the swash and collision regime the mass flux carried by the waves and rollers returns offshore as a return flow or a rip-current. These offshore directed flows keep the erosion process going by removing sand from the slumping dune face. Various models have been proposed for the vertical profile of these currents (see Reniers et al., 2004b, for a review). However, the vertical variation is not very strong during extreme conditions and has been neglected for the moment.

Surf and swash zone sediment transport processes are very complex, with sediment stirring by a combination of short-wave and long-wave orbital motion, currents and breaker-induced turbulence. However, intra-wave sediment transports due to wave asymmetry and wave skewness are expected to be relatively minor compared to long-wave and mean current contributions (Van Thiel de Vries et al., 2008). This allows for a relatively simple and transparent formulation according to Soulsby & Van Rijn (Soulsby, 1997) in a shortwave averaged but wave-group resolving model of surf zone processes. This formulation has been applied successfully in describing the generation of rip channels (Damgaard et al., 2002; Reniers et al., 2004a) and

barrier breaching (Roelvink et al., 2003).

In the collision regime, the transport of sediment from the dry dune face to the wet swash, i.e. slumping or avalanching, is modeled with an avalanching model accounting for the fact that saturated sand moves more easily than dry sand, by introducing both a critical wet slope and dry slope. As a result slumping is predominantly triggered by a combination of infragravity swash runup on the previously dry dune face and the (smaller) critical wet slope.

During the overwash regime the flow is dominated by lowfrequency motions on the time scale of wave groups, carrying water over the dunes. This onshore flux of water is an important landward transport process where dune sand is being deposited on the island and within the shallow inshore bay as overwash fans (e.g. Leatherman et al., 1977; Wang and Horwitz, 2007). To account for this landward transport some heuristic approaches exist in 1D, e.g. in the SBeach overwash module (Larson et al., 2004) which cannot be readily applied in 2D. Here, the overwash morphodynamics are taken into account with the wave-group forcing of low-frequency motions in combination with a robust momentum-conserving drying/flooding formulation (Stelling and Duinmeijer, 2003) and concurrent sediment transport and bed-elevation changes.

Breaching of barrier islands occurs during the inundation regime, where a new channel is formed cutting through the island. Visser (1998) presents a semi-empirical approach for breach evolution based on a schematic uniform cross-section. Here a generic description is used where the evolution of the channel is calculated from the sediment transports induced by the dynamic channel flow in combination with avalanche-triggered bank erosion.

## 1.3 XBeach skillbed

The XBeach code and related functionalities develop fast. As a result there is a need from modelers and code developers to develop a tool that gives insight in the effect of code developments on model performnace. The XBeach skillbed tries to fulfill this need by running a range of tests including analytical solutions, laboratory tests and practical field cases every week with the latest code.

# Chapter 2

# Overview

In the table below, the statuses of all tests found in the skillbed are summarized. The first three colomns identify the test with a combination of a binary, test and run name. The following three columns provide information on the status of that specific run. These columns indicate whether the model ran, the analysis ended succesfully and whether the run used default or custom settings. An empty status means the run or analysis is ignored, a cross indicates failure and a checkmark indicates success. The other columns in the table provide information on the model configuration.

Tests can be run multiple times using different settings. Different runs are identified by a run name, which follows after the test name. If a test runs once only, it is common use to name the run *default*. This is not the same as running a test with default settings, which is indicated in the "Default settings" column.

The table provides all tests ran in a single skillbed run. This report not necessarily uses all available tests. Therefore, not all tests in the table are necessarily found in the continuation of this report.

# Chapter 3

# Hydrodynamic tests

Morphodynamics start with hydrodynamics. In this chapter the hydrodynamic results of XBeach are discussed. All tests are run without the morphological module and the analsyis is focussed on the wave propagation and transformation computed by XBeach.

First, two analytical solutions are reproduced by XBeach. Subsequently, two laboratory experiments are discussed and finally a field experiment.

## 3.1 Long wave propagation

The purpose of the this test is to check if the NSWE numerical scheme is not too dissipative and that it does not create large errors in propagation speed.

A long wave with a small amplitude of $0.01m$ and period of $80s$ was sent into a domain of $5m$ depth, grid size of $5m$ and a length of $1km$. At the end, a fully reflecting wall is imposed. The wave length in this case should be $\sqrt{g \cdot d} \cdot T = \sqrt{9.81 \cdot 5} \cdot 80 = 560m$. The velocity amplitude should be $\sqrt{g/h} \cdot A = \sqrt{9.81/5} \cdot 0.01 = 0.014m$. After the wave has reached the wall, a standing wave with double amplitude should be created.

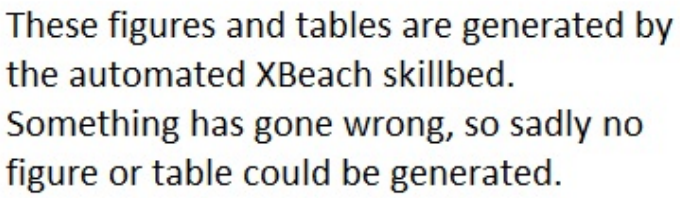


*Figure 3.1: Water levels and velocities from the start of the experiment until the wave just reaches the end of the flume*

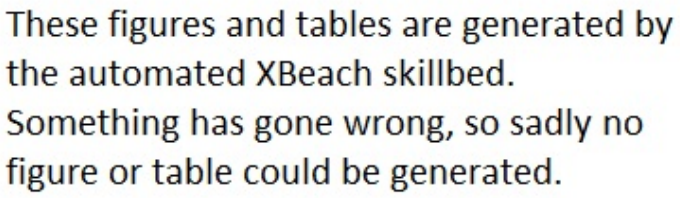


*Figure 3.2: Snapshots of water levels and velocities showing a standing wave pattern*

## 3.2 1D wave runup (analytical solution)

The purpose of this test is to check the ability of the model to represent runup and rundown of non-breaking long waves. To that end, a comparison was made with the analytical solution of the NSWE by Carrier and Greenspan (1958), which describes the motion of harmonic, non-breaking long waves on a plane sloping beach without friction.

A free long wave with a wave period of 32 seconds and wave amplitude of half the wave breaking amplitude ($a_{in} = 0.5 \cdot a_{br}$) propagates over a beach with constant slope equal to $1/25$. The wave breaking amplitude is computed as $a_{br} = 1/\sqrt{128} \cdot \pi^3 \cdot s^{2.5} \cdot T^{2.5} \cdot g^{1.25} \cdot h_0^{-0.25} = 0.0307m$, where $s$ is the beach slope, $T$ is the wave period and $h_0$ is the still water depth at the seaward

boundary. The grid is non uniform and consists of 160 grid points. The grid size $\Delta x$ is decreasing in shoreward direction and is proportional to the (free) long wave celerity ($\sqrt{g \cdot h}$). The minimum grid size in shallow water was set at $\Delta x = 0.1m$.

To compare XBeach output to the analytical solution of Carrier and Greenspan (1958), the first are non-dimensionalized with the beach slope $s$, the acceleration of gravity $g$, the wave period $T$, a horizontal length scale $L_x$ and the vertical excursion of the swash motion $A$. The horizontal length scale $L_x$ is related to the wave period via $T = \sqrt{L_x/g \cdot s}$ and the vertical excursion of the swash motion $A$ is expressed as: $A = a_{in} \cdot \pi/\sqrt{0.125 \cdot s \cdot T \cdot \sqrt{g/h_0}}$

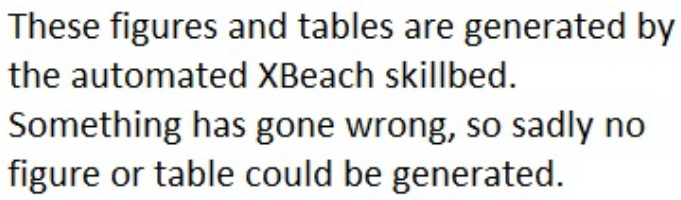


*Figure 3.3: Snapshots of water level and velocity*

## 3.3 2D wave runup

The verification cases so far considered solely the cross-shore dimension and assumed a long-shore uniform coast. In the following case the potential of the model to predict coastal and dune erosion in situations that include the two horizontal dimensions is further examined. A first step towards a 2DH response is to verify that the 2DH forcing by surge run-up and run-down is accurately modelled by testing not against Zelt (1986), but actually Özkan-Haller and Kirby (1997). The reason is that Zelt modeled the NSW equations including some dispersive and dissipative terms, which the present model does not include. For that reason, we compared the model to the results of Özkan-Haller and Kirby (1997) who modeled the NSW equations using a Fourier-Chebyshev Collocation method, which does not have any numerical dissipation or dispersion errors. They use a moving, adapting grid with a fixed $\Delta y$ (which is equal to the present model's $\Delta y$ in this comparison) but with a spatially and temporally varying $\Delta x$ so that the grid spacing in $x$ near the shoreline is very small. In the present model $\Delta x$ is set equal to $\Delta y$, which means that we can expect to have less resolution at the shoreline than Özkan-Haller and Kirby (1997).

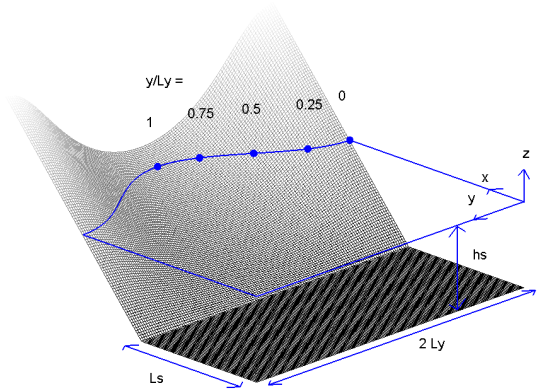


*Figure 3.4: Definition scetch of concave beach bathymetry*

Figure 3.4 shows the definition sketch of the concave beach bathymetry in the present coordinate system, converted from the original system by Zelt (1986). The bathymetry consists of a flat bottom part and a beach part with a sinusoidally varying slope. For Zelt (1986)'s fixed parameter choice of $\sqrt{\beta} = \frac{h_s}{L_y} = \frac{4}{10\pi}$, the bathymetry is given by

$$\mathrm{h} = \{$$

$$\begin{array}{lll} h_s & , & x \leq L_s \\ h_s - \frac{0.4(x-L_s)}{3-\cos\left(\frac{\pi y}{L_y}\right)} & , & x > L_s \end{array}$$

where $h_s$ is the shelf depth, $L_s$ is the length of the shelf in the modeled domain and $L_y$ is the length scale of the longshore variation of the beach. This results in a beach slope of $h_x = \frac{1}{10}$ in the center of the bay and of $h_x = \frac{1}{5}$ normal to the "headlands". In the following we chose $L_y = 8\,m$, which determines $h_s = 1.0182\,m$. We set $L_s = L_y$. Different values for $L_s$ only cause phase shifts in the results, but no qualitative difference, so this parameter is not important in this problem. Also indicated in the figure are the five stations where the vertical run-up (the surface elevation at the shoreline) will be measured.

At the offshore ($x = 0$) boundary we specify an incoming solitary wave, which in dimensional form reads

$$\zeta_i(t) = \alpha h_s \mathrm{sech}^2\left(\sqrt{\frac{3g}{4h_s}\alpha(1+\alpha)}(t-t_o)\right)$$

which is similar to Zelt (1986)'s Eq. (5.3.7). The phase shift $t_o$ is chosen such that the surface elevation of the solitary wave at $t = 0$ is 1% of the maximum amplitude. The only parameter yet to be chosen is $\alpha$. We will compare our model to Zelt's case of $\alpha = \frac{H}{h_s} = 0.02$, where $H$ is the offshore wave height. Zelt found that the wave broke for a value of $\alpha = 0.03$, so the present test should involve no breaking, but has a large enough nonlinearity to exhibit a pronounced two-dimensional run-up.

Any outgoing waves will be absorbed at the offshore boundary by the absorbing-generating boundary condition. At the lateral boundaries $y = 0$ and $y = 2\,L_y$ we specify a no-flux (wall) boundary condition following Zelt (1986). The model equations used in this test are the nonlinear shallow water equations without forcing or friction. The numerical parameters are $\Delta x = \Delta y = \frac{1}{8}\,m$ with a Courant number $\nu = 0.7$.

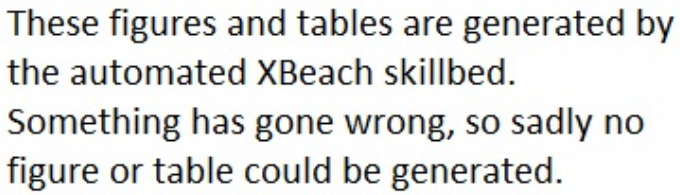


*Figure 3.5: Normalized vertical runup in time (panel 1) and maximum and minimum values (panel 2)*

The first panel in Figure 3.5 shows the vertical runup normalized with the offshore wave height H as a function of time, which is normalized by $\sqrt{g\,h_s}/L_y$ at the 5 cross-sections indicated in Figure 3.4. The solid lines represent the present model results, while the dashed lines denotes Özkan-Haller and Kirby (1997)'s numerical results. The second panel in Figure 3.5 shows the maximum vertical run-up and run-down, normalized by $H$, versus the alongshore coordinate $y$. Table 3.1 presents error statistics of the model run with respect to the measurements.

*Table 3.1: Error statistics Zelt Case 1*

These figures and tables are generated by
the automated XBeach skillbed.
Something has gone wrong, so sadly no
figure or table could be generated.

## 3.4 High- and low-frequency wave transformation

Boers (1996) performed experiments with irregular waves in the physical wave flume at Delft University of Technology with a length of 40 meters and a width of 0.8 m. The flume is equipped with a hydraulically driven, piston type wave generator with second-order wave generation and Active Reflection Compensation. Boers ran waves over a concrete bar-trough beach, which was modelled after the Delta Flume experiments. He ran three different irregular wave conditions, but in this report we will focus on case 1C, a Jonswap spectrum with $H_{m,0} =$ 0.1m and $T_p = 3.3$s. The surface elevation was measured in 70 locations shown in Figure 3.6.

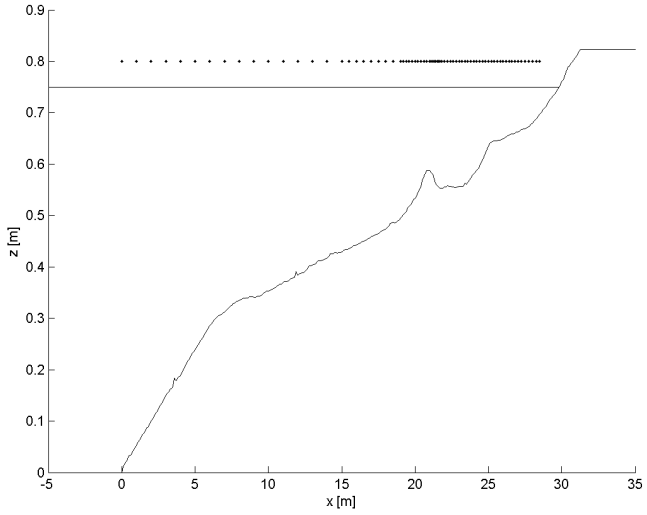


*Figure 3.6: Locations of surface eleveation measurements*

The comparison between the model and the data for the wave height transformation of the short waves and the long waves (defined as waves with a frequency greater than $f_p/2$ and less than $f_p/2$, respectively) is shown in Figure 3.7.

The red dashed line and triangles indicate the short wave height transformation. The blue line and circles indicate the mean (steady) set-up. The dotted red line and upside-down traiangles indicate the total (incoming and reflected) low frequency wave.

The observational data is separated into incoming and reflected long wave components using an array of wave gauges (Bakkenes, 2002) and the numerical data has been separated into two components using co-located surface elevation and velocity information.

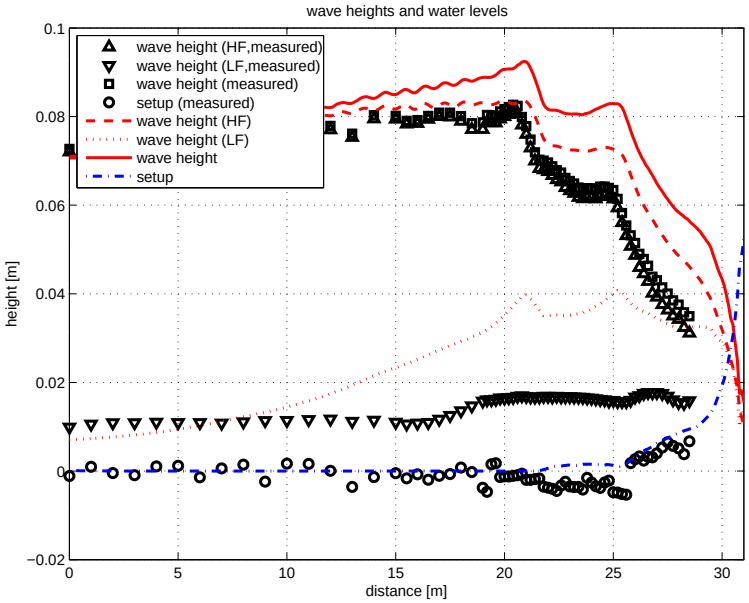


*Figure 3.7: Wave height transformations during Boers 1C experiment*

## 3.5 Field experiment: DELILAH

In order to verify the 2DH hydrodynamics of XBeach when forced by directionally-spread short waves, a simulation is set up to compare model results to field measurements. In this case the DELILAH field experiment at Duck, North Carolina is selected as a suitable test location. The period that is modeled is October 13th 1990, which was a stormy day, between 16:00 and 17:00 hours. The significant wave height at 8 m water depth was 1.81 m, with a peak period of 10.8 s and a mean angle of incidence of -16$^o$ relative to the shoreward normal. This period is selected because the wave conditions are energetic enough to generate a significant infragravity wave component and the incident wave spectrum is sufficiently narrow-banded to justify the assumptions in the model boundary conditions. The model is forced with the wave spectrum measured at 8 m water depth (Birkemeier et al., 1997). A measured tidal signal is imposed on the model boundaries of which the mean level is 0.69 m above datum. The slope of the wave front in the roller model is set to 0.05, which is found to be a slight improvement over the value of 0.10 used in the previous sections. A constant grid size of 5 m in cross shore and 10 m in longshore direction is used. The resolution of the wave model in directional space is 15$^o$. The model is set to generate output at the location of the primary cross shore measurement array, gauge numbers 10, 20, 30, 40, 50, 60, 70, 80 and 90 (Figure 3.8).

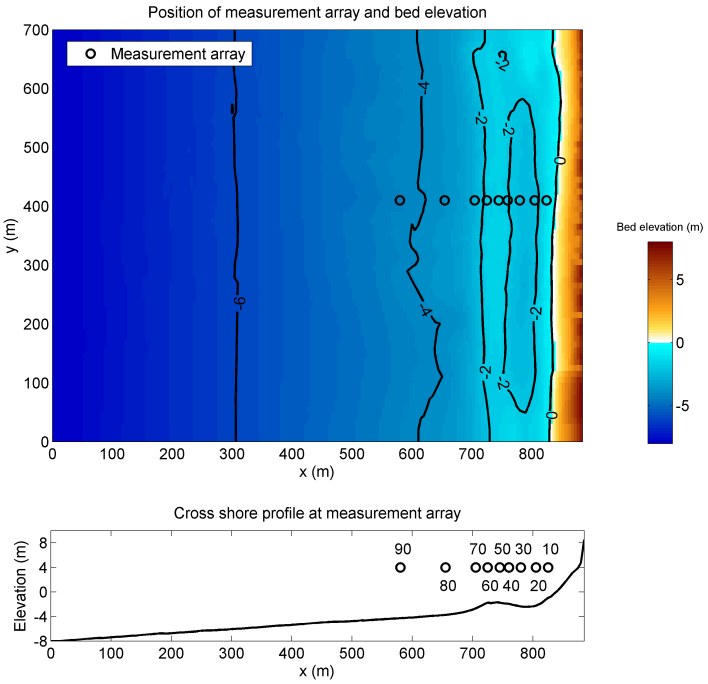


*Figure 3.8: Bathymetry and measurement locations*

The modeled time-averaged wave heights of the short waves are compared to the time-averaged wave heights measured at the gauges. These results are shown in the first panel of Figure 3.9. Unfortunately, no data exist for gauge number 60.

The infragravity wave height is calculated as follows (Van Dongeren et al., 2003):

$$H_{rms,low} = \sqrt{8 \int_{0.005Hz}^{0.05Hz} S df}$$

Figure 3.9 shows the infragravity wave height. The measured and modelled time-averaged longshore current are shown in the second panel of Figure 3.9. The correlation coefficient, scatter index, relative bias and Brier Skill Score for the simulation are shown in Table 3.2.

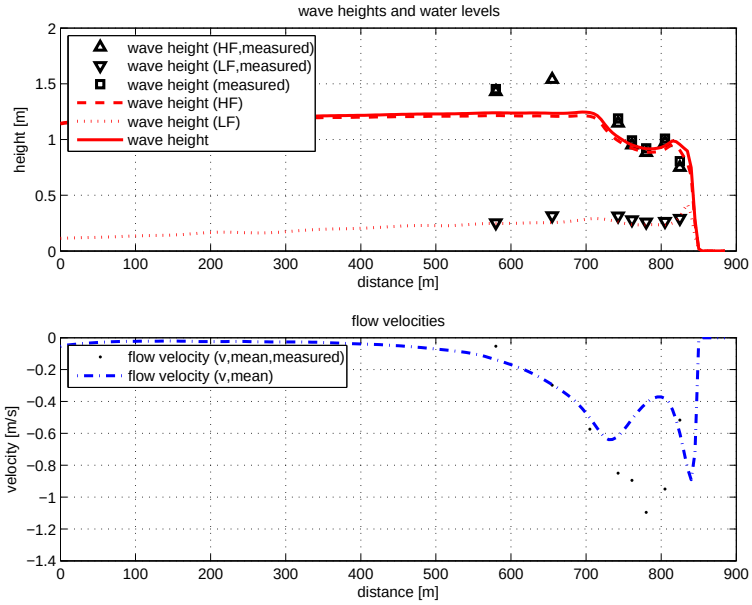


*Figure 3.9: Wave height transformation and flow velocities during the DELILAH field experiment 1990*

*Table 3.2*

| | $R^2$ | Sci | Rel. bias | BSS |
|---|---|---|---|---|
| $Hrms_lf$ | 0.70 | 0.13 | -0.12 | 0.50 |
| $Hrms_hf$ | 0.94 | 0.15 | -0.12 | 0.76 |
| $vmean$ | 0.69 | 0.46 | 0.28 | 0.43 |

The modeled and measured sea surface elevation spectra at four gauge locations are shown in Figure 3.10. Note that the modeled surface elevation spectra only contain low frequency components associated with wave groups.

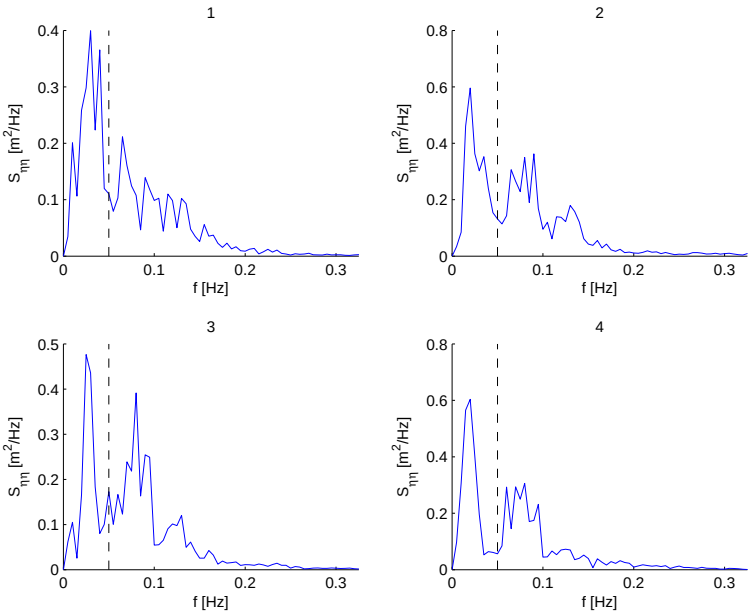


*Figure 3.10: Modelled surface elevation spectra for four locations in the primary cross shore array during the DELILAH field experiment 1990*

## 3.6 Field experiment: Ningaloo reef

Ningaloo Reef is a large fringing reef on the northwest coast of Australia and consists of a series of reef-channel cells, exposed to tropical cyclones and Southern Ocean swells. A field data set of wave transformation on a shore-normal transect (Figure 3.11) taken at Sandy Bay in June 2009 is described in (Pomeroy et al., 2012). The transect is composed of a steep fore reef, a shallow reef flat ( $1-2m$ depth) that is separated from the shore by a slightly deeper lagoon ( $2-3m$ average depth). Instrument C1 was deployed on the forereef slope, C3 and C4 were located on the reef flat, while C5 and C6 were located inside the lagoon behind the reef. The wave field exhibits a dramatic decay in the incident swell band on the fore reef section with a transfer of part of the energy to infragravity waves which are dissipated due to bottom friction over the reef flat and lagoon.

The XBeach model formulations have been extended with a friction dissipation term in the wave action equation (Dongeren et al. (2013), which also describes the following case). For this site, optimum friction coefficient values ($f_w = 0.6$, $c_f = 0.1$) were determined for a 1D version of the model based on conditions at the peak of the swell event. These settings were subsequently used to simulate the entire swell event from June 14 12:00 hours to June 19 00:00 hours (109 hours in total) when wave conditions varied significantly. Good agreement was generally observed throughout the simulation and at all sites (**??**; Figure 5 in Dongeren et al. (2013)). The model reproduced the spatial variability in wave heights across the reef, as well as temporal changes in the response to the varying offshore wave conditions and tidal variations. The short wave height predictions matched the data reasonably well (Figure 3.12 a-e), except for a small positive bias of a few centimeters. The IG wave heights were slightly under predicted (negative bias) at C1, but were generally in very good agreement for sites on the reef (Figure 3.12 f-j). The time series of the predicted mean water level residuals (the time-averaged difference between the observed water level on the reef and the observation at C1, $\overline{\Delta z_s} = \overline{z_s - z_{s,C1}}$, thus describing wave setup) followed the observed residuals reasonably well, albeit that the model over predicts the observations by about 0.1 m. (Figure 3.12 l-o)

Note that at C1 the observed and predicted water levels rather than the residuals are shown (**??** k). A summary of the model skill (bias and the RMS error) for the short wave heights, IG heights and mean water level is shown in Figure 3.13 (Figure 6 in Dongeren et al. (2013)).

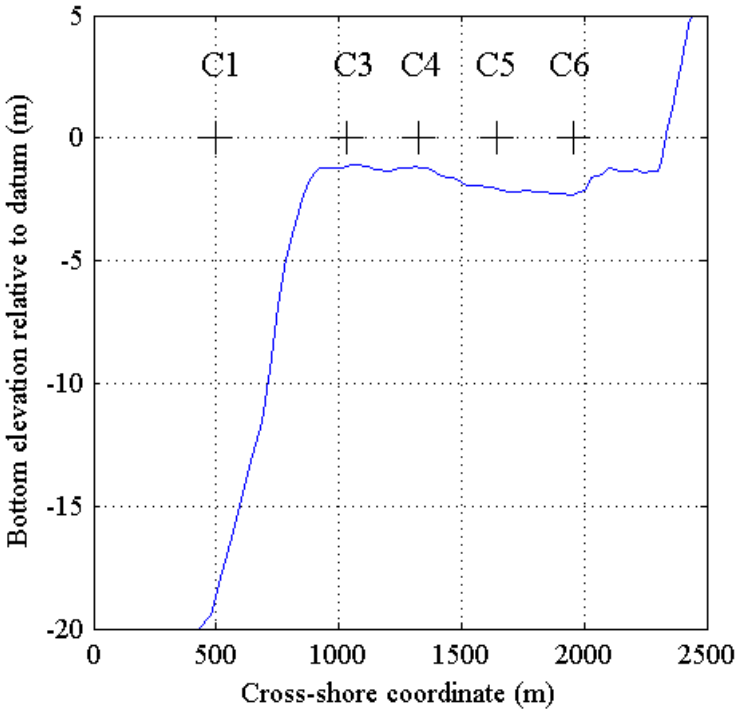


*Figure 3.11: Cross-shore profile of the bathymetry along the main measurement transect with instrument locations shown.*

These figures and tables are generated by the automated XBeach skillbed.
Something has gone wrong, so sadly no figure or table could be generated.

*Figure 3.12: Comparison between the 1D model results (blue) and measured data (red) for the duration of the 5 day swell event. (a,f,k) are for instrument C1, (b,g.l) C3, (c,h,m) C4, (d,i,n) C5 and (e,j,o) C6. The peak of the storm is indicated by the red vertical line. Note the large reduction in vertical scale between C1 and the reef sites C3-C6.*

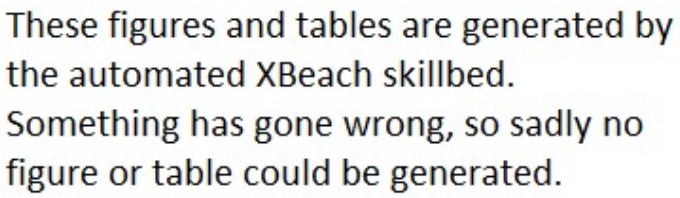


*Figure 3.13: Bias and RMS error from the 1D swell duration ( 5 day) model results compared with the measured data at each site, based on the short wave heights, IG wave heights, and mean water levels.*

## 3.7 Longcrested refraction

Longcrested waves are supported in XBeach by using a value s larger than 1,000. The directional distribution in that case is a spike corresponding to the mean wave direction. Due to the discretization in the wave directional dimension, numerical diffusion in this dimension may occur. In case of a narrow directional distribution, the numerical diffusion may lead to a loss of wave energy through the boundaries of the directional grid.

To limit the numerical directional diffusion, the directional grid may be chosen with large grid cells and thus decreasing the gradients between adjacent grid cells. Directional advection may be turned of entirely when using a single directional grid cell, since refraction is not possible with a single grid cell at all. However, when using oblique longcrested waves in a 2DH model, none of these solutions suffice.

This test shows the numerical directional diffusion in the comparison of a few runs where the angle of wave incidence and the number of directional bins vary. The bathymetry is a linear sloping beach and no morphological change is computed in these runs.

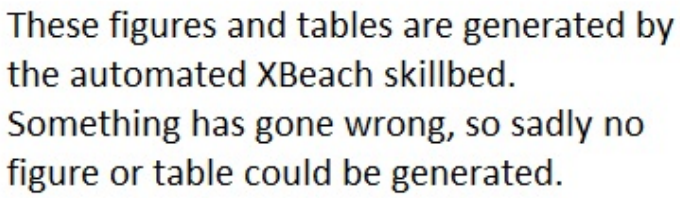


*Figure 3.14: Wave height*

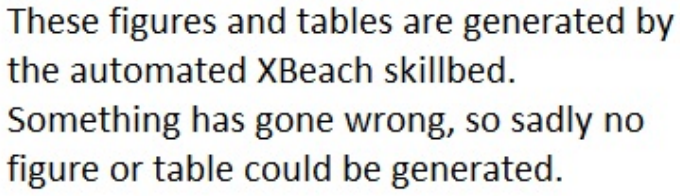


*Figure 3.15: Mean wave direction*

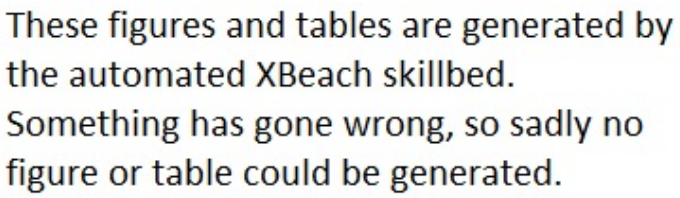


*Figure 3.16: Time-averaged wave forcing in lateral direction*

This test is to check the refraction behaviour of loncrested waves, which are simulated using instat=stat and m=1000. Four cases are generated and compared: directional bins of 2.5, 5 and 10 degrees and a single bin. In all cases the incident wave angle is 60 degrees and theta grid runs from -10 to 90 degrees. The results are compared among themselves and, for the wave direction, with Snel's law and with mean direction computed by integrating $c_\theta/c_{g,x}$ over x. The results all agree within approx. one degree, whch is considered satisfactory. Note that the longshore current does not exhibit any negative velocities, as was noticed when the refraction is not computed correctly.

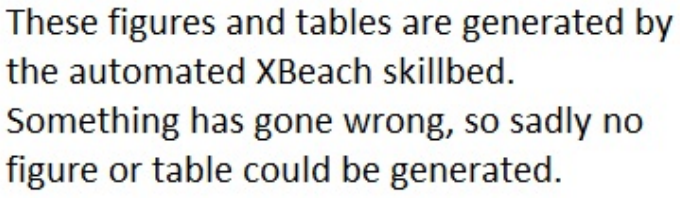


*Figure 3.17: Wave energy, direction and flow velocities for different sized of theta bins.*

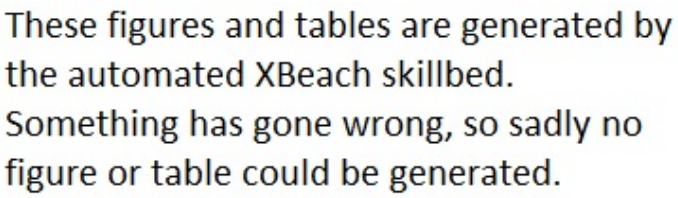


*Figure 3.18: Refraction with different sizes of theta bins. The red dotted line indicates the solution according to Snel law.*

## 3.8 Tide

This test was set up to verify the capability of XBeach to model tidal elevation and longshore currents in a small model, based on water level time series at the seaward corner points, which have a small time shift. The current pattern should spin up in a longshore uniform pattern and remain longshore uniform at all times. In the figure velocity patterns at six times during a one-day simulation are shown. Also the input timeseries of water levels at the corners (dots) can be compared with the model water

level time series, which should closely follow the input but may have a small delay depending on the type of boundary condition chosen (abs_1d, abs_2d or waterlevel) and on settings of epsi (-1 in this case) and cats (5). In this case without wave forcing, the abs_2d boundary type does not perform well; water levels do not match the input. This is probably due to the absence of waves. With abs_1d the results as in the reference figure are shown.

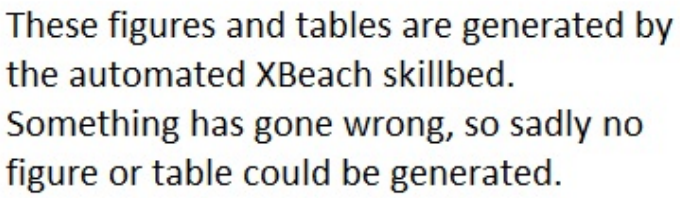


*Figure 3.19: The lower-left panel shows the tidal timeseries imposed to the offshore corners of the model (dots) and the generated waterlevels at these locations (lines). For six moments indicated with the black vertical lines, the flow field is shown in the upper panels.*

### 3.8.1 Blankenberge

This represents a realistic test model of the coast and port of Blankenberge on the Belgian coast, in a model set up by IMDC and Flanders Hydraulics. The model experienced bad tidal currents; after fixing this problem the accompanying figure show smooth and realistic current patterns with a nearshore current dominated by wave-driven currents (instationary, JONSWAP-type, with waves from 270 degrees, so a large angle to the coast. In this case the abs_2d boundary option does not pose a problem to the tidal forcing. In the present setup we run it with theta bins of 20 degrees.

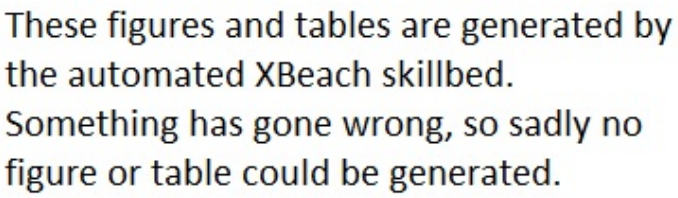


*Figure 3.20: The lower-left panel shows the tidal timeseries imposed to the offshore corners of the model (dots) and the generated waterlevels at these locations (lines). For six moments indicated with the black vertical lines, the flow field is shown in the upper panels.*

# Chapter 4

# Morphological laboratory tests

In this chapter, the performance of XBeach is compared to results obtained from physical model tests performed in a variety of laboratory facilities. Many of those tests are part of fundamental research into dune erosion and other morhpological processes. Research took place on different scales, mainly depending on the size of the facility used. A key issue in laboratory research is the translation of the laboratory results to the prototype situation, which often requires scale relations.

The first section of this chapter covers an important measurement campaign commissioned by the Dutch Ministry of Public Works in order to derive these scale relations. The following sections cover in-depth analysis of other laboratory tests and research to bar evolution, interactions with structures and other specific processes.

## 4.1 Scale relations

During the 1953 storm surge, large areas in the western part of the Netherlands were inundated. This catastrophic event urged the Dutch Government to initiate fundamental research to sea defences in general and dunes in particular. In the Netherlands, a major part of the sea defence consists of dunes. The aim of the government was to make all sea defences withstand a storm surge with a once in 10,000 years frequency of occurance.

In order to maintain this newly introduced norm, fundamental research to dune erosion was necessary. A key issue in this field of research was the translation from laboratory results to prototype situations. Therefore, the Ministry of Public Works commisioned a research campaign in order to derive scale relations that facilitate this translation. Many experiments with a variety of scales, sediments and hydraulic conditions are performed in this context between 1974 and 1981. The experiments are presented in three parts: exploring experiments on small scale, additional experiments on small scale and verification experiments on a large scale. The three parts are discussed in the following subsections.

In contrast to models that are currently used for the assessment of dunes in The Netherlands, XBeach is a process based model. If a process based model describes the relevant processes of dune erosion (on different scales) accurately, it should be capable of reproducing the entire series of tests in this research campaign. In order to verify whether XBeach is capable hereof, the measurement results are compared to the XBeach results in the following subsections.

During all experiments described in this section, the reference profile for the Holland coast

is used. This profile is a schematized profile that is considered representative for the Holland coast.

### 4.1.1 Small scale tests

From 1974 to 1975, 58 model experiments for the derivation of scale relations are performed in the Wind Flume of Laboratory De Voorst in the Netherlands (Van de Graaff, 1976). Four different depth scales are used in these experiments: 150, 84, 47 and 26. Also, two different sediment diameters are used: 225$\mu$m and 150$\mu$m. During all experiments, the dune is exposed to a significant wave height of 7.6m and a constant maximum surge level of 5m+NAP on prototype scale.

*Table 4.1: Overview of experiments*

| Experiment | Scale | Profile contraction | Sediment diameter | Water depth | Wave height | Wave period |
|---|---|---|---|---|---|---|
| BT13 | 84 | 9 | 150 | 0.461 | 0.091 | 1.31 |
| CT14 | 84 | 9 | 225 | 0.461 | 0.091 | 1.31 |
| BT15 | 84 | 7 | 150 | 0.461 | 0.091 | 1.31 |
| CT16 | 84 | 7 | 225 | 0.461 | 0.091 | 1.31 |
| BT17 | 84 | 5 | 150 | 0.461 | 0.091 | 1.31 |
| CT18 | 84 | 5 | 225 | 0.461 | 0.091 | 1.31 |
| BT23 | 47 | 7 | 150 | 0.585 | 0.163 | 1.76 |
| CT24 | 47 | 7 | 225 | 0.585 | 0.163 | 1.76 |
| BT25 | 47 | 5 | 150 | 0.585 | 0.163 | 1.76 |
| CT26 | 47 | 5 | 225 | 0.585 | 0.163 | 1.76 |
| BT27 | 47 | 3 | 150 | 0.585 | 0.163 | 1.76 |
| CT28 | 47 | 3 | 225 | 0.585 | 0.163 | 1.76 |
| AT33 | 26 | 3 | 150 | 0.806 | 0.292 | 2.35 |
| DT34 | 26 | 3 | 225 | 0.806 | 0.292 | 2.35 |
| AT35 | 26 | 1.5 | 150 | 0.806 | 0.292 | 2.35 |
| DT36 | 26 | 1.5 | 225 | 0.806 | 0.292 | 2.35 |
| AT37 | 26 | 5 | 150 | 0.806 | 0.292 | 2.35 |
| DT38 | 26 | 5 | 225 | 0.806 | 0.292 | 2.35 |
| AT61 | 84 | 5 | 150 | 0.461 | 0.091 | 1.31 |
| BT62 | 84 | 5 | 150 | 0.461 | 0.091 | 1.31 |
| CT63 | 84 | 7 | 225 | 0.461 | 0.091 | 1.31 |
| DT64 | 84 | 5 | 225 | 0.461 | 0.091 | 1.31 |
| AT71 | 26 | 3 | 150 | 0.806 | 0.292 | 2.35 |
| BT71 | 17 | 2.6 | 150 | 0.806 | 0.292 | 2.35 |
| CT71 | 26 | 3 | 225 | 0.806 | 0.292 | 2.35 |
| DT71 | 26 | 3 | 225 | 0.806 | 0.292 | 2.35 |
| AT91 | 47 | 3 | 150 | 0.806 | 0.292 | 1.76 |
| BT92 | 26 | 3 | 150 | 0.806 | 0.292 | 1.76 |
| CT93 | 26 | 3 | 225 | 0.806 | 0.292 | 1.76 |
| DT94 | 26 | 4 | 225 | 0.806 | 0.292 | 1.76 |
| AT95 | 47 | 3 | 150 | 0.806 | 0.163 | 2.35 |
| BT96 | 47 | 4 | 150 | 0.806 | 0.163 | 2.35 |
| CT97 | 26 | 3 | 225 | 0.806 | 0.163 | 2.35 |
| DT98 | 47 | 3 | 225 | 0.806 | 0.163 | 2.35 |

The flume had a length of approximately 100m and a width of 4m. The flume was subdivided in four parts with a width of 1m each. Using this configuration, it was possible to perform four experiments at a time. All experiments are therefore considered to be one-dimensional.

Among the 58 experiments available, 6 experiments were calibration experiments, another 6 experiments are performed on a very small scale (150), in 4 experiments the profile development was disturbed and in another 8 experiments a variable surge comparable with the 1953 storm surge was used. These experiments are excluded from the skillbed as for now. The 34 experiments left are presented in Table 4.1.

The profile development computed by XBeach is compared to the measurements for all 34 experiments. One of these comparisons is shown in Figure 4.1. For all other experiments, only the resulting Brier Skill Score is presented in Figure 4.2.

*Figure 4.1*

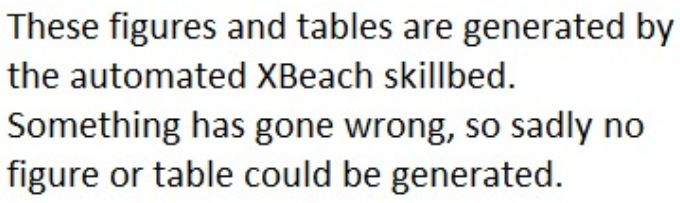


*Figure 4.2: Overview of Brier Skill Scores*

### 4.1.2 Additional small scale tests

The experiments presented in the previous section resulted in a set of scale relations (Van de Graaff, 1976). Moreover, the experiments indicated that the process of dune erosion scaled with the dimensionless parameter $\frac{H}{T \cdot w}$. In order to verify these findings, a series of additional small scale tests is performed in 1976 and 1977 (Vellinga, 1981). Again, the Wind Flume of Laboratory De Voorst in The Netherlands was used.

During the additional experiments, only the depth scales 84, 47 and 26 are used. The sediment diameter is varied between 95$\mu$m and 225$\mu$m. Tests with constant and varying waterlevels are performed. Here, only the tests with constant water levels are considered. XBeach is compared to all tests performed on scale 26 plus the tests on the scales 84 and 47 for which a sediment diameter of 225$\mu$m was used. These tests are summarized in Table 4.2.

*Table 4.2: Overview of experiments*

| Experiment | Scale | Profile contraction | Sediment diameter | Water depth | Wave height | Wave period |
|---|---|---|---|---|---|---|
| 111 | 84 | 4.0 | 225 | 0.461 | 0.091 | 1.31 |
| 115 | 84 | 2.9 | 225 | 0.461 | 0.091 | 1.31 |
| 101 | 47 | 3.4 | 225 | 0.585 | 0.163 | 1.76 |
| 105 | 47 | 2.5 | 225 | 0.585 | 0.163 | 1.76 |
| 121 | 26 | 3.0 | 225 | 0.806 | 0.292 | 2.35 |
| 122 | 26 | 2.0 | 225 | 0.806 | 0.292 | 2.35 |
| 123 | 26 | 2.2 | 150 | 0.806 | 0.292 | 2.35 |
| 124 | 26 | 1.5 | 150 | 0.806 | 0.292 | 2.35 |
| 125 | 26 | 1.6 | 130 | 0.806 | 0.292 | 2.35 |
| 126 | 26 | 1.1 | 130 | 0.806 | 0.292 | 2.35 |
| 127 | 26 | 1.3 | 95 | 0.806 | 0.292 | 2.35 |
| 128 | 26 | 1.0 | 95 | 0.806 | 0.292 | 2.35 |

Figure 4.3 shows the profile comparison of one of the tests from Table 4.2. For the other tests, the Brier Skill Score is presented in Figure 4.4.

*Figure 4.3*

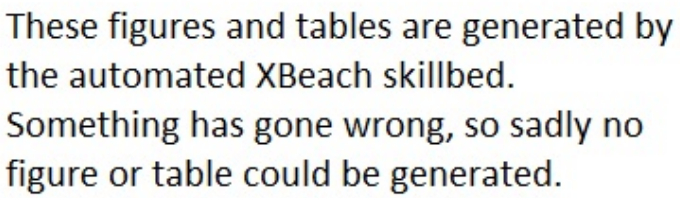


*Figure 4.4: Overview of Brier Skill Scores*

### 4.1.3 Large scale tests

The experiments presented in the previous sections (Van de Graaff, 1976; Vellinga, 1981), resulted in a final theory on scale relations and the translation of small scale results to prototype situations (Vellinga, 1986). In order to verify this theory, large scale model tests are performed in 1980 and 1981 in the Deltaflume of Delft Hydraulics, currently known as

Deltares (Vellinga, 1984). The Deltaflume is approximately 230m long, 5m wide and 7 to 9m deep.

Five experiments are performed, as presented in Table 4.3. Tests 1, 2 and 5 had a constant surge level, while tests 3 and 4 had a variable surge level with a course depicted in Figure 4.5 and Figure 4.6 respectively.

*Table 4.3: Overview of experiments*

| Experiment | Scale | Profile contraction | Sediment diameter | Water depth | Wave height | Wave period |
|---|---|---|---|---|---|---|
| 1 | 5 | 1.91 | 225 | 4.2 | 1.50 | 5.4 |
| 2 | 5 | 1.27 | 225 | 4.2 | 1.50 | 5.4 |
| 3 | 5 | 1.27 | 225 | 4.2 | 1.50 | 5.4 |
| 4 | 3.27 | 1.91 | 225 | 4.2 | 1.85 | 5.0 |
| 5 | 1 | 1 | 225 | 5.0 | 2.00 | 7.6 |

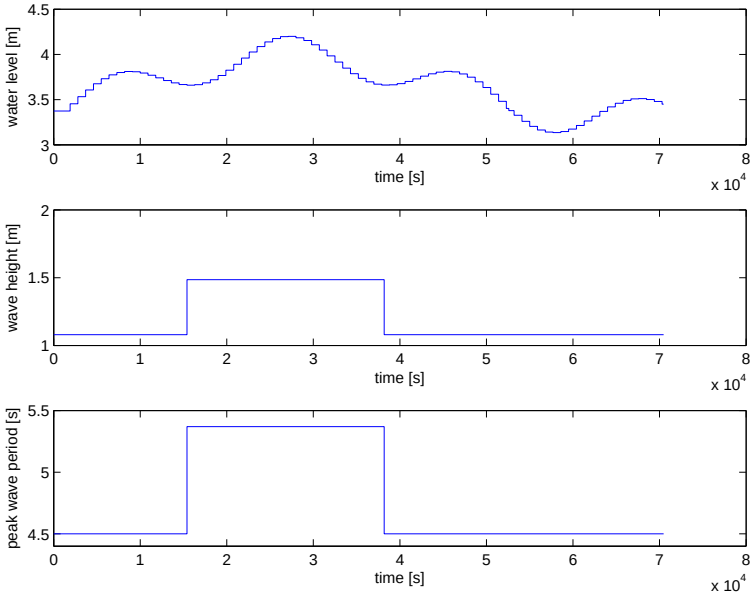


*Figure 4.5: Boundary conditions for test 3*

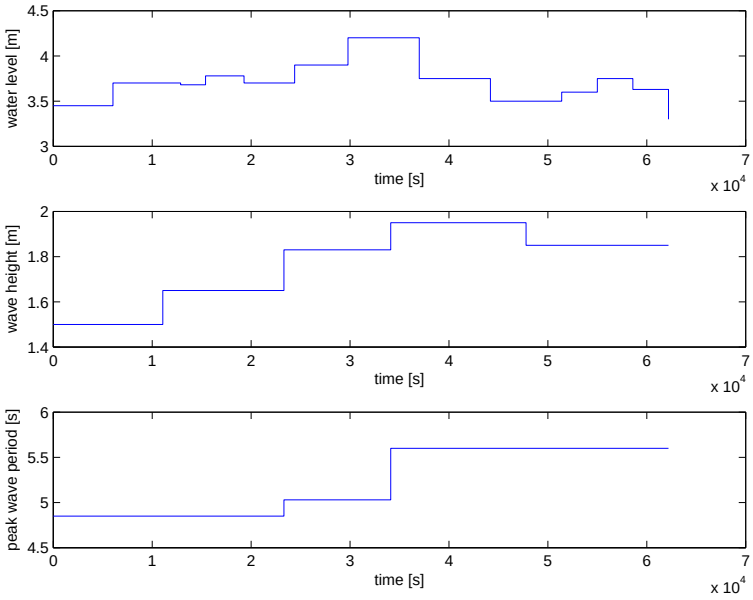


*Figure 4.6: Boundary conditions for test 4*

As in the previous sections, the profile developments are compared to the measurements in Figure 4.7 to Figure 4.11. Moreover, erosion patterns and volumes and retreat distances are analyzed in Figure 4.13 to Figure 4.17. Figure 4.12 provides an overview of the Brier Skill Scores of the profile development for the different tests.

These figures and tables are generated by the automated XBeach skillbed.
Something has gone wrong, so sadly no figure or table could be generated.

*Figure 4.7: Profile development during test 1*

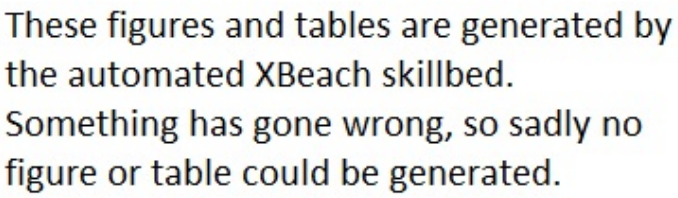


*Figure 4.8: Profile development during test 2*

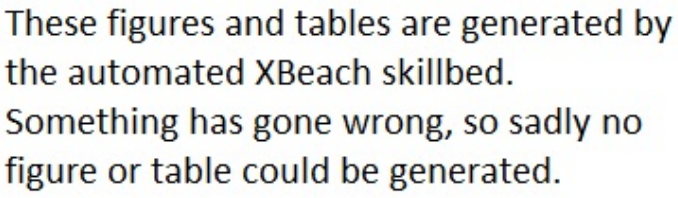


*Figure 4.9: Profile development during test 3*

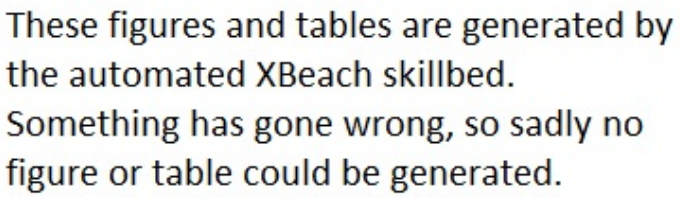


*Figure 4.10: Profile development during test 4*

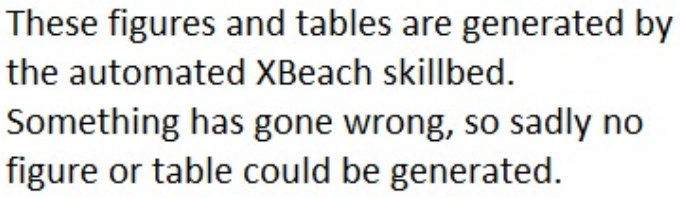


*Figure 4.11: Profile development during test 5*

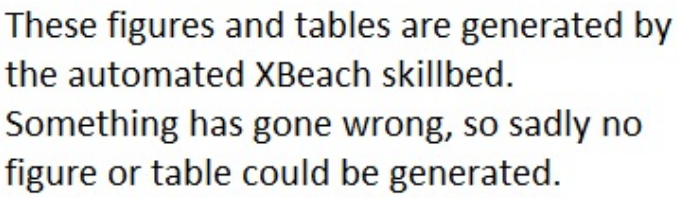


*Figure 4.12: Overview of Brier Skill Scores*

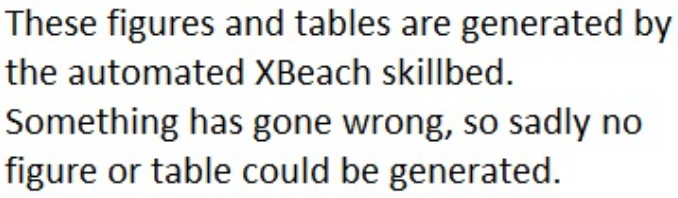


*Figure 4.13: Development of erosion volumes during test 1*

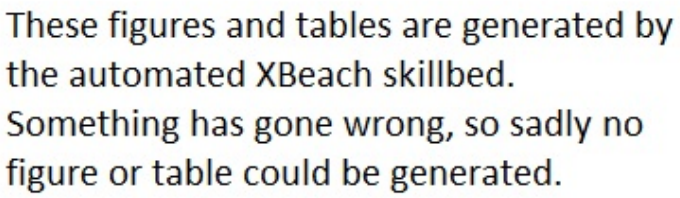


*Figure 4.14: Development of erosion volumes during test 2*

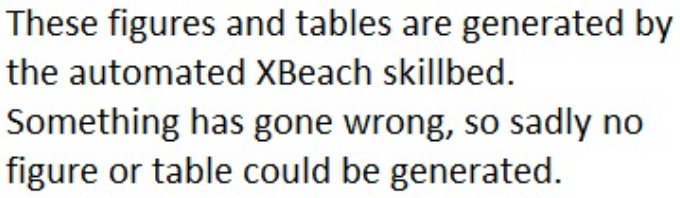


*Figure 4.15: Development of erosion volumes during test 3*

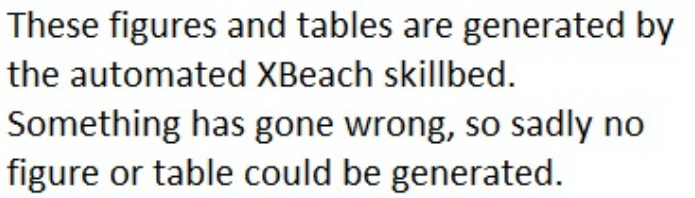


*Figure 4.16: Development of erosion volumes during test 4*

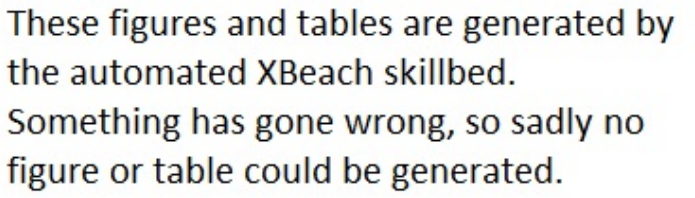


*Figure 4.17: Development of erosion volumes during test 5*

## 4.2 Large scale tests

This section discusses a selection of large scale laboratory experiments. The experiments focus on specific situations and processes that XBeach is assumed to model well.

### 4.2.1 Revetments

Revetments or other hard structures influence the dune erosion process. Scour holes and wave runup on structures can occur, both important phenomena in the assessment of water defences. Scour holes are mainly caused due to the obstructed transport of sediments in seaward direction from the dune. A transport gradient causes a scour hole to occur. This is

also valid for other hard elements present in or near a dune. (Short) wave runup can cause overtopping of the revetment, which can cause erosion at the rear-side of the revetment.

#### 4.2.1.1 Influence of reventment height

Steetzel (1987) describes a series of large scale experiments with revetments of different heights. The experiments are performed in the Deltaflume of Delft Hydraulics, now known as Deltares. A depthscale $n_d = 5$ is used for all experiments (Vellinga, 1986) and the initial profile in the flume correponds to the reference profile for the Holland coast. At the dune foot, which was located at 193m from the wave board and 3.80m above the flumes floor, a concrete revetment is applied that covers almost the whole dune face with a slope of 1:1.8. The lower end of the revetment is located at 2.5m above the flume floor. The location of the top of the revetment varied in each experiment. The tests were conducted with a constant water level of 4.2m and wave conditions that correspond to a Pierson-Moskowitz spectrum with $H_{m0} = 1.50$m and $T_p = 4.20$s. The sediment applied in the test had a median grain diameter of approximately $D_{50} = 210\mu$m. An overview of the tests is given in Table 4.4.

*Table 4.4: Overview of experiments*

| Experiment | Revetment height w.r.t. flume floor |
|---|---|
| T1 | 6.20m |
| T2 | 5.40m |
| T3 | 4.80m |

The profile developments as measured and computed by XBeach are presented in Figure 4.18 to Figure 4.20.

These figures and tables are generated by the automated XBeach skillbed. Something has gone wrong, so sadly no figure or table could be generated.

*Figure 4.18: Profile development during test T1*

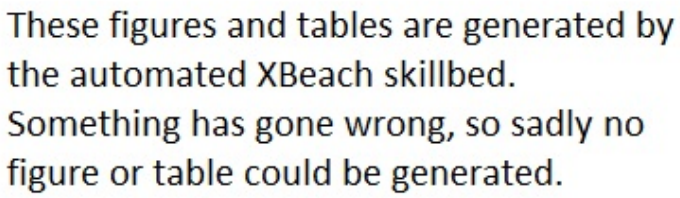


*Figure 4.19: Profile development during test T2*

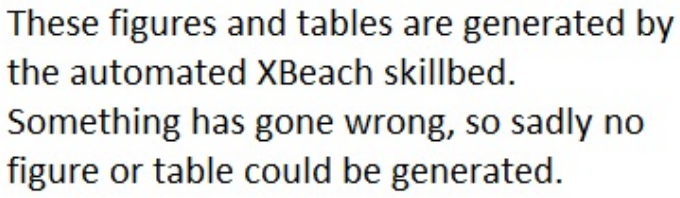


*Figure 4.20: Profile development during test T3*

### 4.2.2 Extreme conditions

This model test, described in Arcilla et al. (1994) (2E), concerns extreme conditions with a raised water level at 4.6m above the flume bottom, a significant wave height, $H_{m0}$, of 1.4m and peak period, $T_p$, of 5s. Bed material consisted of sand with a $D_{50}$ of approximately 0.2mm. During the test substantial dune erosion took place.

Based on the integral wave parameters $H_{m0}$ and $T_p$ and a standard Jonswap spectral shape, time series of wave energy were generated and imposed as boundary condition. Since the flume tests were carried out with first-order wave generation (no imposed super-harmonics and sub-harmonics), the hindcast runs were carried out with the incoming bound long waves set to zero as well. Active wave reflection compensation (ARC) was applied in the physical model, which has a result similar to the weakly reflective boundary condition in XBeach,

namely to prevent re-reflecting of outgoing waves at the wave paddle (offshore boundary).

A grid resolution of 1m was applied and the sediment transport settings were set at default values. For the morphodynamic testing the model was run for 0.8 hours of hydrodynamic time with a morphological factor of 10, effectively representing a morphological simulation time of 8 hours.

In Figure 4.21 the hydrodynamic results are shown for first order wave generation (as in the flume tests).

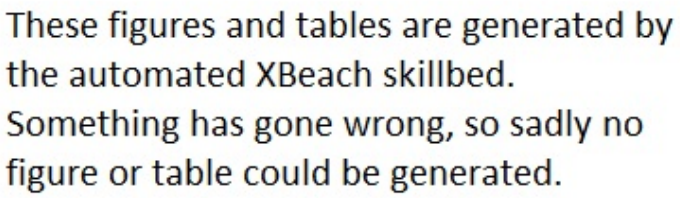


*Figure 4.21: Hydrodynamics during test 2E*

In Figure 4.22 the horizontal distribution of sedimentation and erosion after 8 hours is shown, and the evolution in time of the erosion volume and the dune retreat. Noteworthy is the episodic behaviour of the dune erosion, both in measurements and model. An important conclusion for physical model tests is that for dune erosion it does make a difference whether first-order or second-order wave steering is applied.

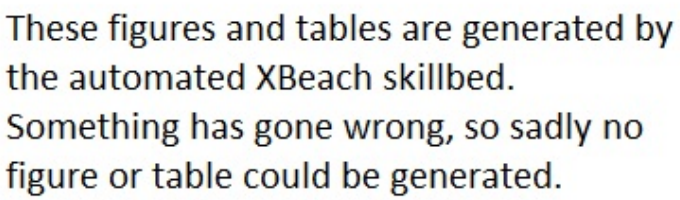


*Figure 4.22: Morphodynamics during test 2E*

A key element in the modelling is the avalanching algorithm; even though surfbeat waves running up and down the upper beach are fully resolved by the model, without a mechanism to transport sand from the dry dune face to the beach the dune face erosion rate is substantially underestimated. The relatively simple avalanching algorithm implemented, whereby an underwater critical slope of 0.3 and a critical slope above water of 1.0 are applied, proves to be quite successful in representing the retreat of the upper beach and dune face. In Figure 4.23 the measured and modelled bed evolution are shown.

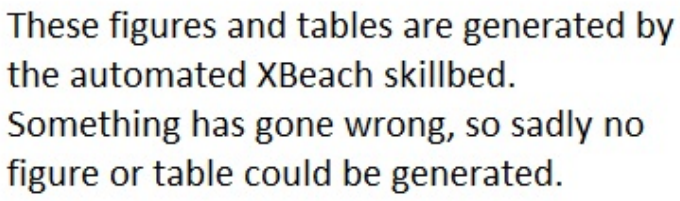


*Figure 4.23: Profile development during test 2E*

### 4.2.3 Bar evolution

In Arcilla et al. (1994) two types of profiles and three different dynamic states are investigated: near-equillibrium, erosive and accretive. Also, a test with extreme erosive conditions is performed. In this section the erosive and accretive tests for the first profile are discussed: test 1B and 1C. The two tests are intended to simulate the erosive effects during a storm and the restoring effects afterwards. A clear dune front is absent in the profile used, only a gently sloping beach is present. In Table 4.5 the conditions of these two tests are summarized.

*Table 4.5: Overview of experiments*

| Experiment | $H_{m0}$ | $T_p$ | Water level | Duration |
|---|---|---|---|---|
| 1B | 1.4m | 5s | 4.1m | 18h |
| 1C | 0.6m | 8s | 4.1m | 13h |

In Figure 4.24 and Figure 4.25 the computed and measured hydrodynamics are shown.

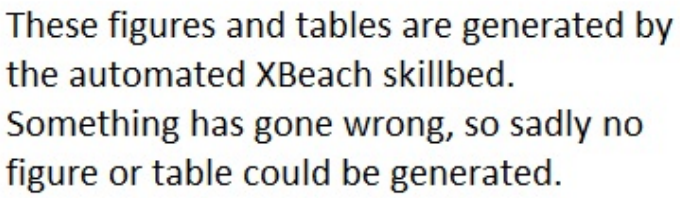


*Figure 4.24: Hydrodynamics during test 1B*

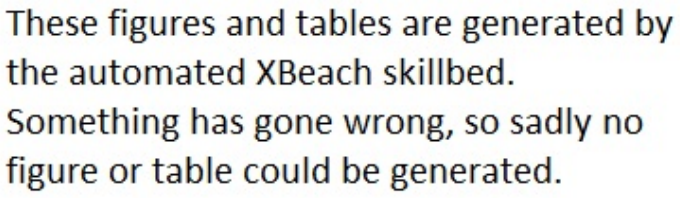


*Figure 4.25: Hydrodynamics during test 1C*

The profile development is shown in Figure 4.26 and Figure 4.27.

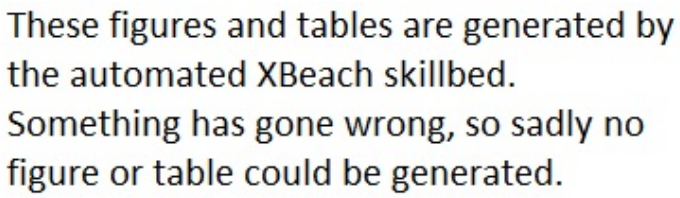


*Figure 4.26: Profile development during test 1B*

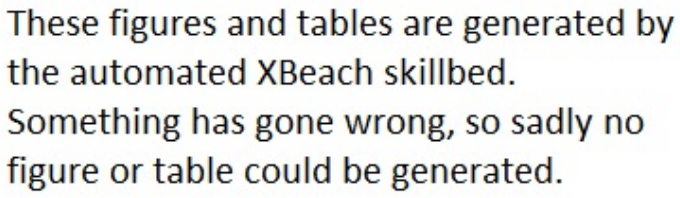


*Figure 4.27: Profile development during test 1C*

### 4.2.4 Influence of wave period

In Van Gent et al. (2008) and Van Thiel de Vries et al. (2008) describe large-scale laboratory experiments on the influence of the wave period on the dune erosion process. It was concluded that not only short waves, but also (wave group generated) long waves are important in the dune erosion process. Initially, about 30% of the dune erosion is due to long wave energy, but this amount increases with the development of an erosion profile. Moreover, an increase of the wave period increases the dune erosion volumes.

XBeach, being a wave group solving model, is expected to be able to reproduce the observed influence of the wave period well. The following sections provide an in-depth comparison of the first experiment from Van Gent et al. (2008). It continue with a comparison of the influence of the wave period and spectrum shape between the measurements obtained and

the XBeach results.

All experiments are performed in the Deltaflume of Delft Hydraulics, currently known as Deltares, using the reference profile for the Holland coast. This is a schematized profile that is considered representative for the Holland coast. Furthermore, a significant wave height 1.50m and a water depth of 4.50m is used. The test programme is given in Table 4.6. During test T04 a profile with a double dune row is used.

*Table 4.6: Overview of experiments*

| Experiment | $T_p$ | $T_{m-1,0}$ | Spectrum |
|---|---|---|---|
| T01 | 4.90 | 4.45 | Pierson-Moskowitz |
| T02 | 6.12 | 5.56 | Pierson-Moskowitz |
| T03 | 7.35 | 6.68 | Pierson-Moskowitz |
| T04 | 7.35 | 6.68 | Pierson-Moskowitz |
| DP01 | 6.12 | 3.91 | double-peaked |
| DP02 | 7.35 | 5.61 | double-peaked |

#### 4.2.4.1 Detailed analysis

In this section, a detailed comparison between simulated physics over an evolving bathymetry and the measurements obtained during the Deltaflume experiment in 2006 (Van Gent et al., 2008) is made. For brevity this comparison is performed only for test T01 (this test corresponds best to the Dutch normative conditions). The simulations are performed on a regular grid with dx = 1m and input to the model are time series of short wave varying energy (low pass filtered on the wave group time scale) and incoming (bound) long waves. The time series are constructed from pressure and flow measurements at x = 41m from the wave board. The short wave group velocity (associated with advection of wave action) is based on the $T_{m-1,0}$ wave period. Other model settings can be found in Van Thiel de Vries (2009).

Wave height transformation and wave setup (Figure 4.43) are favourably reproduced with the model. The long wave height is slightly underestimated whereas the wave setup is slightly overestimated. The correlation between measured short wave variance and long wave water surface elevations (Figure 4.29) corresponds reasonably well with the measurements. Towards the shoreline this correlation increases (Abdelrahman and Thornton, 1987; Roelvink and Stive, 1989) meaning the highest short waves travel on top of long waves, which likely causes that more short wave energy gets closer to the dune face.

Short wave skewness and asymmetry are reasonably predicted with the extended Rienecker Fenton model (Figure 4.30, panel 1). However, in the inner surf zone both wave skewness and asymmetry are overestimated. Possible explanations are wave breaking, which limits the steepness and height of waves and the presence of free harmonics in the flume. Both these effects are not included in the wave shape model but indeed are present in the flume test (Van Thiel de Vries, 2009). From simulated skewness and asymmetry it follows that the total nonlinearity of a short wave is overestimated close to the dune face (Figure 4.30, panel 2). The phase $\beta$ is favourably simulated with the model but is underestimated further offshore.

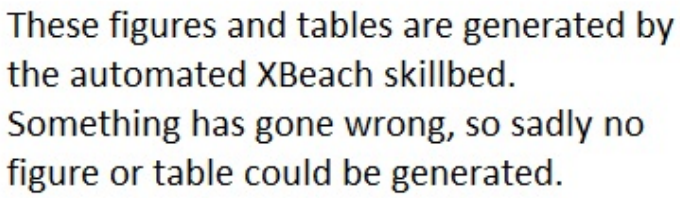


*Figure 4.28: Wave height transformations and flow velocities*

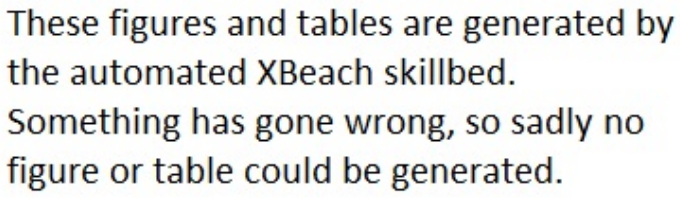


*Figure 4.29: Correlation between short wave variance and long wave surface elevations*

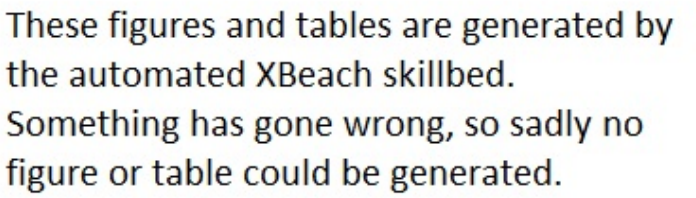


*Figure 4.30: Wave shape and nonlinearity*

The simulated test and depth averaged flow velocity shows the same trend as in the measurements and increases towards the shoreline (Figure 4.31). However, in the simulation the cross-shore range with a high offshore mean flow is smaller and extends less far seaward than in the measurements. This is possibly explained by differences in profile development (Figure 4.37) or inaccurate measurements. In addition, another explanation may be found in the incorrect modeling of the roller energy dissipation. Simulations (not shown) with a smaller roller dissipation rate revealed that roller energy in the inner surf increases, leading to higher return flow over a broader cross-shore range.

Long waves contribute to the time and depth averaged flow close to the shoreline. The contribution of long waves to the mean flow is explained by on average larger water depths during the interval associated with shoreward flow velocities in relation to the interval with offshore flow velocities. Considering continuity and a uniform vertical structure of the long wave flow this means a time and depth averaged offshore directed flow should be present.

Nonlinear waves may cause onshore sediment transport presuming non-uniform sediment stirring over the wave cycle and a positive correlation between sediment suspension and the intra wave flow. In order to include the wave averaged effect of nonlinear waves on the sediment transport a mean flow $u_A$ is computed, which is added to the mean (Eulerian) flow $U_m$ (Van Thiel de Vries, 2009). The simulated time averaged flow associated with nonlinear waves shows a comparable evolution as in the measurements but is overestimated especially closer to the dune face. Near the shoreline the wave skewness related sediment transport vanishes (Figure 4.30, panel 1) since waves develop towards fully saw tooth shaped bores that have negligible skewness.

The orbital flow velocity (Figure 4.43, panel 2) is favourably predicted by the model. The short wave orbital flow velocity is slightly overestimated whereas the long wave orbital flow is underestimated. The underestimation of the simulated long wave orbital flow corresponds well to the slight underestimation of the observed long wave water surface variance.

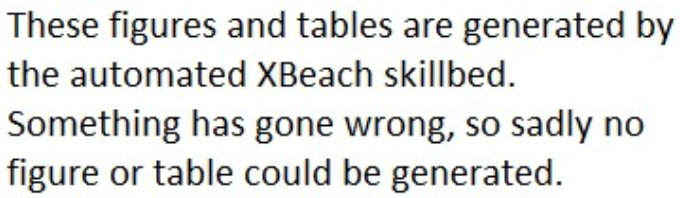


*Figure 4.31: Wave motion velocities and undertow*

The simulated test and depth averaged sediment concentration increases towards the shoreline but is underestimated, especially in deeper water where the modeled sediment concentration is smaller (Figure 4.32). In the proximity of the dune face the simulated mean sediment concentration is within a factor two with the measurements. Further offshore the discrepancy between simulations and measurements is larger. The sharp rise in the near dune sediment concentration compares well with the bore averaged near-bed turbulence intensity (Figure 4.33) that also increases towards the shoreline. This increase in turbulence intensity through the inner surf is explained by more intensive wave breaking (turbulence pro-duction at the water surface increases) and by decreasing water depth (generated turbulence at the water surface is more effective in reaching the bed).

The simulated time averaged sediment transport compares well with the measured sediment transport computed from profile changes (Figure 4.34, panel 1). Sediment is eroded from the dune face via avalanching and as a result the sediment transport associated with avalanching is dominant over the dune face and in the swash zone. From the swash zone seaward, the flow based sediment transport becomes more important. At 205m from the wave board, in a water depth that varies between 0.1m and 0.2m, the flow related sediment transport is dominant.

The simulated flow related sediment transport is separated in sediment transports as-ociated with nonlinear waves ($S_W$), long waves ($S_L$) and the short wave driven under-tow ($S_R$) (Figure 4.34, panel 2):

$S_W = \overline{u_A ch}$

$S_L = \overline{u^L ch}$

$S_R = \overline{(u^E - u^L) ch}$

The offshore sediment transport results from the short wave and roller driven under-tow ($S_R$) combined with the transport associated with the long waves ($S_L$). The transport that follows from the short wave undertow is dominant in the present simu-lation but the long wave related sediment transport cannot be neglected (about 30% at the location of the maximum offshore transport). The wave related sediment transport ($S_W$) is onshore and suppresses the offshore sediment transport with some 30%.

Profile evolution and dune erosion volumes are favourably predicted with the model during test T01 (Figure 4.37 and Figure 4.40, panel 2). Between t = 2.04 and 6.0 hours (interval E) the dune erosion rate is slightly underestimated. At the offshore edge of the developing foreshore, the model seems not capable to reproduce the steep transition from the original (unaffected) profile towards the newly developed foreshore. A bar type feature is observed at this transition that is hypothesized to be related to (partly) plunging breakers that generate a water jet, which penetrates in the water column and causes additional sediment stirring when it reaches the bed. Though the effect of wave breaking induced turbulence on sediment suspension is included in the simulation, the applied model only considers spilling breakers, which are expected to be less efficient than plunging breakers in stirring up sand.

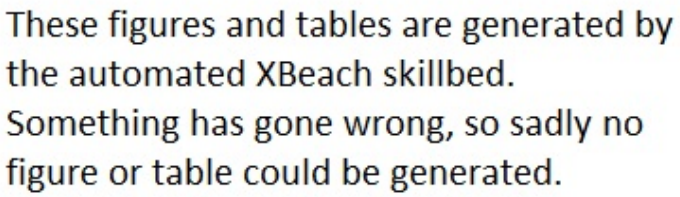


*Figure 4.32: Sediment concentrations*

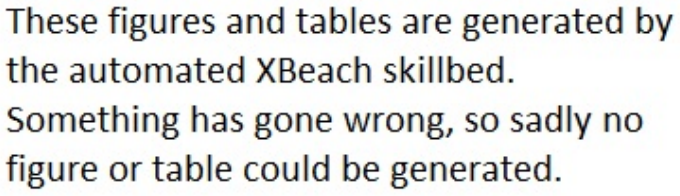


*Figure 4.33: Wave induced turbulence*

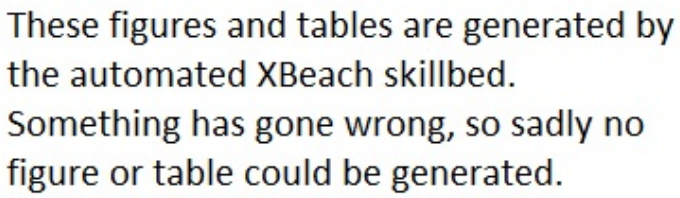


*Figure 4.34: Sediment transports by transport type and forcing*

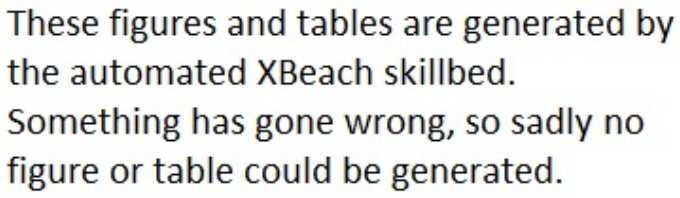


*Figure 4.35: Profile development*

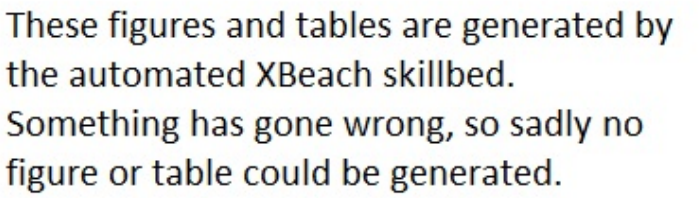


*Figure 4.36: Bed level changes and erosion volumes*

It is concluded that profile evolution and dune erosion during test T01 are favourably simulated. Also simulated wave heights, flows, sediment concentrations and sediment transports compare reasonably well with measurements. However,looking at the results in more detail some discrepancies are found:

1. The long wave height and especially associated long wave orbital flows are un-derestimated.
2. The test and depth averaged flow between x = 170 m and x = 200 m is underestimated. Close to the shoreline no reliable measurements are available to verify the model results.
3. The simulated sediment concentration compares well with measurements close to the dune face. However, for smaller sediment concentrations in deeper water the simulated concentration is underestimated.
4. The offshore sediment transport is mainly driven by the short wave and roller induced undertow (O(70%) at the location of the maximum offshore transport) whereas the offshore directed long wave related sediment transport cancels out with the onshore sediment transport due to nonlinear short waves.

It is remarked that shoreward of the maximum offshore sediment transport, the importance of the long wave related transport increases and eventually becomes dominant in relation to the transport associated with short wave and roller driven undertow. Considering the mainly long wave associated sediment transport in proximity of the dune face and the importance of long wave run-up for avalanching it is expected that long waves are mainly responsible for the swash zone sediment transport.

An overview of the Model Performance Statistics for test T01 with respect to the measurements is given in Table 4.7.

*Table 4.7: Model Performance Statistics for test T01*

These figures and tables are generated by the automated XBeach skillbed. Something has gone wrong, so sadly no figure or table could be generated.

#### 4.2.4.2 Wave period

During test T01, T02 and T03 of the 2006 Deltaflume experiment (Van Gent et al., 2008) the effect of the wave period on dune erosion was examined. It was found that the dune erosion volume increases for a larger wave period, which is caused by a larger flow related sediment transport. In addition, the increase in flow related sediment transport is mainly a result of a higher mean sediment concentration whereas the time and depth averaged flow velocity has the same order of magnitude within the range of wave periods examined.

The aim of this section is to examine the processes, which cause the wave period effect in the model and to what extent these processes are in line with the mechanisms observed in the measurements. To this end test T01, T02 and T03 of the Deltaflume experiment are simulated. The simulations are performed on a regular grid with dx = 1 m and input to the model are time series of short wave varying energy (low pass filtered on the wave group time scale) and incoming (bound) long waves. The time series are constructed from pressure and flow measurements at x = 41 m from the wave board. The short wave group velocity (associated with advection of wave action) is based on the $T_{m-1,0}$ wave period. Settings for the wave energy dissipation model are found in Table 4.8 and other setting are defaults as listed in in Appendix B in Van Thiel de Vries (2009).

*Table 4.8: Wave dissipation parameter settings*

| Experiment | $\alpha$ | $\gamma$ | $n$ |
|---|---|---|---|
| T01 | 1.0 | 0.50 | 10 |
| T02 | 1.0 | 0.48 | 10 |
| T03 | 1.0 | 0.45 | 10 |

In Figure 4.37 to Figure 4.39 the simulated profile evolution during the tests compares well with the measured profile evolution. However, the bar type feature at the offshore edge of the developing foreshore is not reproduced in the simulations. Comparing measured and simulated dune erosion volumes in Figure 4.40 to Figure 4.42 it is seen that for test T03 the erosion volume after 1 hour and 2.04 hours of waves is underestimated whereas for test T01 and T02 simulated erosion volumes are reasonably well predicted over all test intervals.

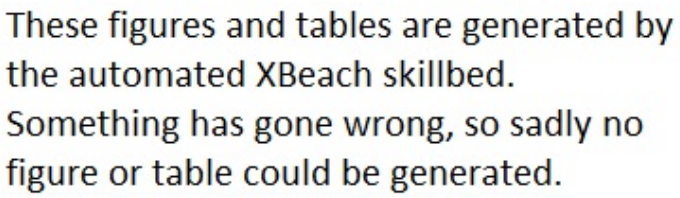


*Figure 4.37: Profile development during test T01*

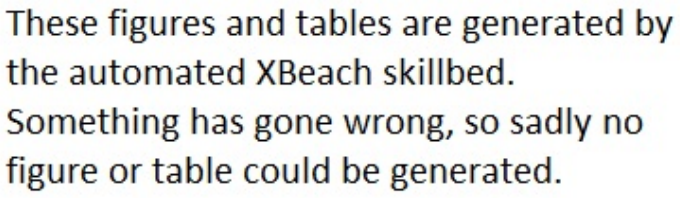


*Figure 4.38: Profile development during test T02*

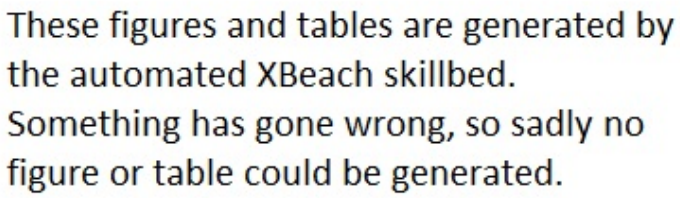


*Figure 4.39: Profile development during test T03*

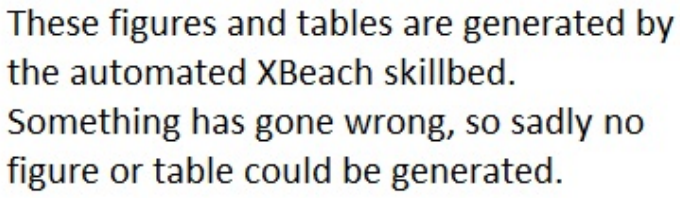


*Figure 4.40: Erosion pattern and volumes and retreat distance during test T01*

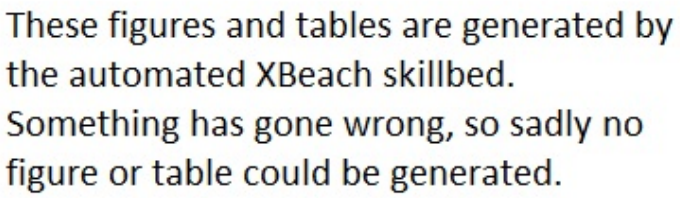


*Figure 4.41: Erosion pattern and volumes and retreat distance during test T02*

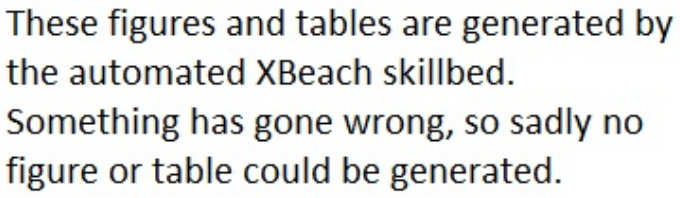


*Figure 4.42: Erosion pattern and volumes and retreat distance during test T03*

Simulated time and depth averaged flows are compared in Figure 4.43 to Figure 4.45, which shows that the mean flow slightly increases with a larger wave period (6% between x = 170 m and x = 205 m). This tends to be a slightly different trend than observed in the measurements that show a 3% increase in the same cross-shore area. It is remarked though that any firm conclusions cannot be made since the measured time and depth averaged flow velocities are based on limited sensors over depth (and for that reason it was concluded that the mean flows for test T01 and T03 are comparable).

The increase in the simulated offshore directed mean flow is caused by an increase of the short wave related mass flux whereas the roller related mass flux is only slightly different. The maximum long wave related mean flow is larger during test T01 than during test T03.

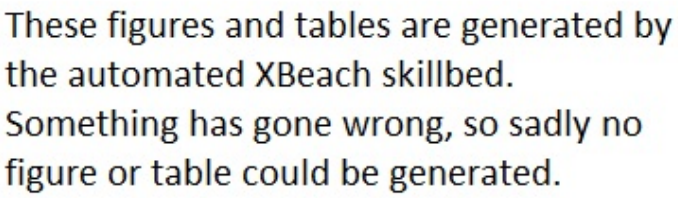


*Figure 4.43: Hydrodynamics during test T01*

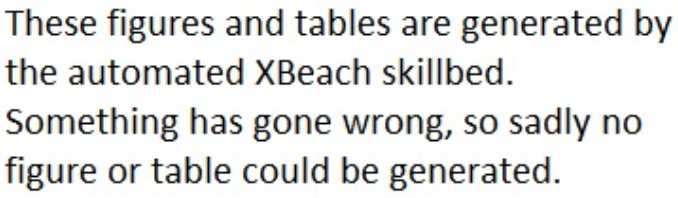


*Figure 4.44: Hydrodynamics during test T02*

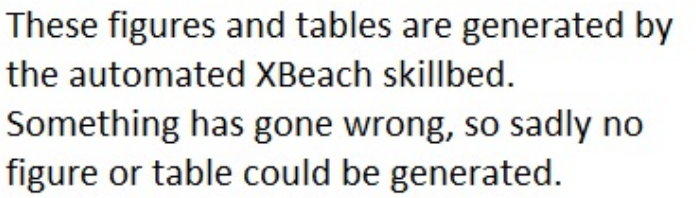


*Figure 4.45: Hydrodynamics during test T03*

It is concluded that the effect of the wave period on dune erosion and dune face retreat is favourably predicted with the XBeach model. The simulated increase in dune erosion with a larger wave period is mainly caused by an increase of the mean sediment concentration of O(60%), which is comparable to the measurements. The near dune return flow slightly increases with approximately 6% for a larger wave period. However, the accuracy of measured time and depth averaged flows is insufficient to verify this increase.

#### 4.2.4.3 Spectral shape

Test DP01 and DP02 were conducted with a double-peaked wave spectrum to investigate what (spectral) wave period is best qualified to describe dune erosion (Van Gent et al., 2008). In this document the tests are discussed to obtain further insight in the capability of the model to simulate dune erosion for various wave spectra. The simulations are performed on a regular grid with dx = 1m and input to the model are time series of short wave varying energy (low pass filtered on the wave group time scale) and incoming (bound) long waves. The time series are constructed from pressure and flow measurements at x = 41 m from the wave board. The short wave group velocity (associated with advection of wave action) is based on the $T_{m-1,0}$ wave period. Settings for the wave energy dissipation model are found in Table 4.9.

*Table 4.9: Wave dissipation parameter settings*

| Experiment | $\alpha$ | $\gamma$ | $n$ |
|---|---|---|---|
| DP01 | 1.0 | 0.50 | 10 |
| DP02 | 1.0 | 0.48 | 10 |

Simulated and measured profile evolution and dune erosion volumes for test DP01 and DP02 are compared in Figure 4.46 to Figure 4.49 respectively. For test DP01 the profile evolution is accurately reproduced and results for test DP02 are reasonable even though the erosion rate during the last interval is overestimated.

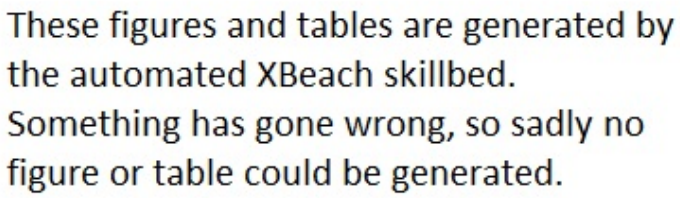


*Figure 4.46: Profile development during test DP01*

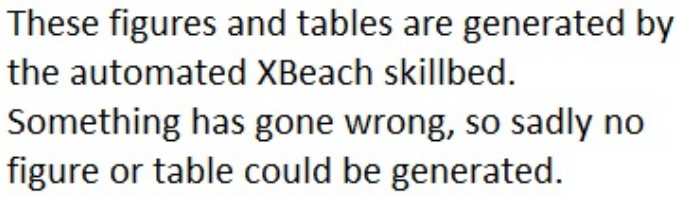


*Figure 4.47: Profile development during test DP02*

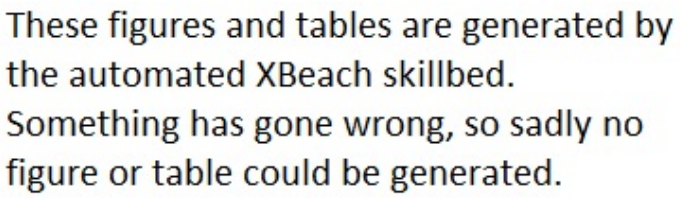


*Figure 4.48: Erosion pattern and volumes and retreat distance during test DP01*

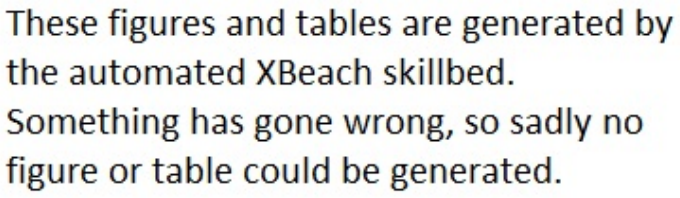


*Figure 4.49: Erosion pattern and volumes and retreat distance during test DP02*

The imposed double-peaked wave spectra affect the time scale and amplitude of the simulated wave groups. Consequently, the interaction of simulated long waves with the short wave groups is different and hydrodynamics in front of the dune face are expected to have other characteristics. In Figure 4.50 and Figure 4.51 the simulated wave transformation, flows and sediment concentrations are favourably compared with measurements obtained during test DP01. It seems the model is capable to take into account the effect of various wave spectra on near dune hydrodynamics and sediment transports.

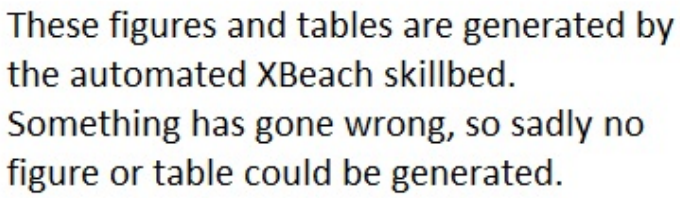


*Figure 4.50: Hydrodynamics during test DP01*

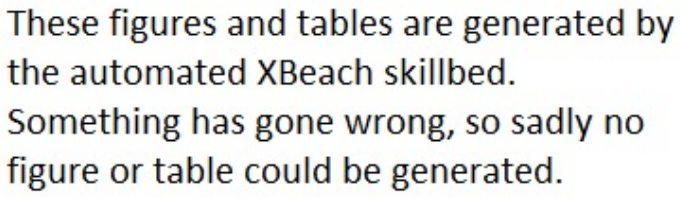


*Figure 4.51: Hydrodynamics during test DP02*

It is concluded that the effect of the wave spectral shape on dune erosion and dune face retreat is favourably predicted with the model. The time averaged simulated wave transformation, flow and sediment concentration compare well with the mobile frame measurements obtained during test DP01.

In Van Gent et al. (2008) the spectral mean wave period $T_{m-1,0}$ is argued to be more qualified to describe dune erosion than the peak wave period $T_p$. The simulations presented in this subsection are performed with the $T_{m-1,0}$ wave period and show satisfying results suggesting the spectral mean wave period proposed by Van Gent et al. (2008) is indeed a good measure to describe dune erosion. It is remarked though that any firm conclusion would require extra simulations in which the peak wave period $T_p$ is applied instead of the $T_{m-1,0}$ wave period. In addition this would demand for a new model optimization and most likely different settings for the wave dissipation model.

#### 4.2.4.4 Double dune system

Test T04 of the Deltaflume experiment 2006 (Van Gent et al., 2008) is carried out with an initial profile that contains a small dune in front of a larger volume dune that collapses after approximately one hour of waves (interval C and D). After breaching of the small dune, the foreshore is already very efficient in reducing wave impacts on the dune face resulting in small erosion rates over the remaining test intervals. In this test it is examined to what extent the dune breach can be reproduced with the XBeach model and whether the (substantially smaller) erosion rate at the end of a storm is correctly predicted. The simulations is performed on a regular grid with dx = 1 m and input to the model are time series of short wave varying energy (low pass filtered on the wave group time scale) and incoming (bound) long waves. The time series are constructed from pressure and flow measurements at x = 41 m from the wave board. The short wave group velocity (associated with advection of wave action) is based on the $T_{m-1,0}$ wave period. Settings for the wave energy dissipation model are equal to the settings for the T03 test.

Simulated profile evolution and dune erosion volumes are shown in Figure 4.52 and Figure 4.53 respectively. The simulated hydrodynamics are presented in Figure 4.54. For the first three intervals (the small dune breaches in interval 3) the dune erosion rate is slightly overestimated but the profile evolution compares favourably with the measured profiles. Considering the last two intervals, erosion rates and dune face retreat are too large.

Breaching of a small dune in front of a larger volume dune causes that suddenly the foreshore is significantly closer to equilibrium with the storm surge conditions. As a result near shore hydrodynamics, near shore sediment transports and wave impacts on the dune face are less severe. It is concluded that the feedback between profile evolution and near dune processes is not sufficiently well included in the model at the end of test T04, which is representative for conditions at the end of a storm. More insight in the model performance at the end of a storm could possibly be obtained by comparing the evolution of simulated driving processes (undertow, sediment concentrations and avalanching) with measurements.

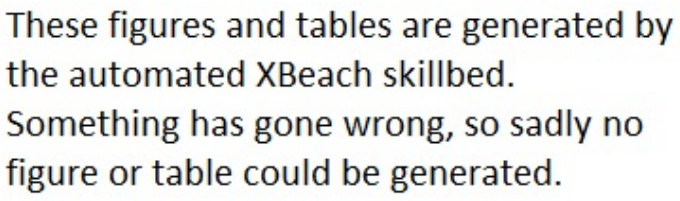


*Figure 4.52: Profile development during test T04*

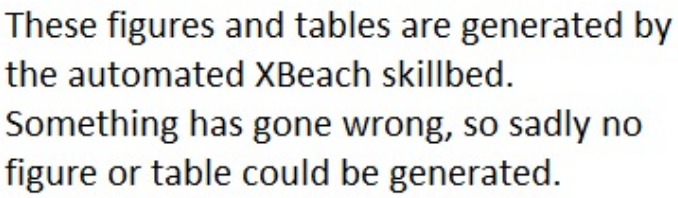


*Figure 4.53: Erosion pattern and volumes and retreat distance during test T04*

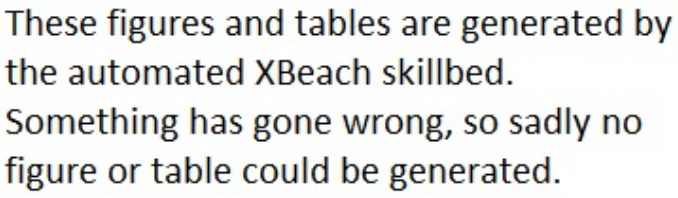


*Figure 4.54: Hydrodynamics during test T04*

# Chapter 5

# Morphological field tests

In this chapter, XBeach is compared to a variety of measurement results obtained from the field. This involves major storm events from the past as well as more moderate situations where morphological behavior is monitored. In general, these tests can be seen as example applications of the XBeach model.

## 5.1 1953 storm surge

In order to test the model performance in prototype conditions, this test studies the impact of the 1953 storm surge on the Dutch coast at Delfland. The initial profile for the simulation is obtained from test T4 of the M1263-III experiment conducted in the Deltaflume (Vellinga, 1984) and is scaled-up to prototype. The profile is representative for the coast at Delfland. The applied grid is uniform with dx = 4.56 m and the applied hydrodynamic conditions vary over the storm (see Figure 5.1). Simulation settings are default except for the maximum erosion rate dzmax, which is scaled-up to $0.17 m^3/ms$ applying the scale relation for the erosion volume (Vellinga, 1986).

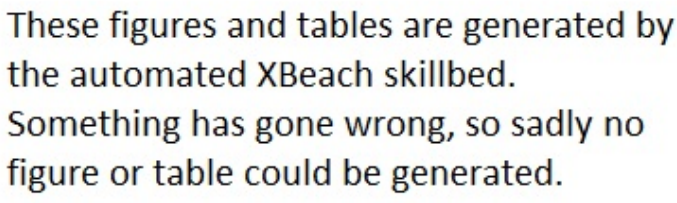


*Figure 5.1: Surge and wave conditions during the 1953 storm surge*

The simulated profile evolution is shown in Figure 5.2. Evolution of the simulated dune erosion volume is shown in Figure 5.3.

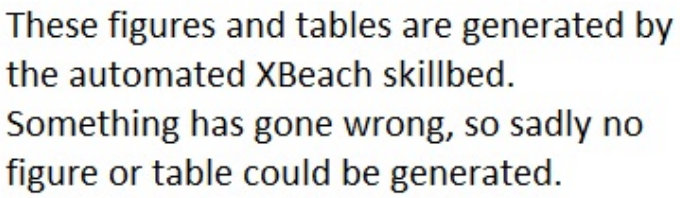


*Figure 5.2: Profile development*

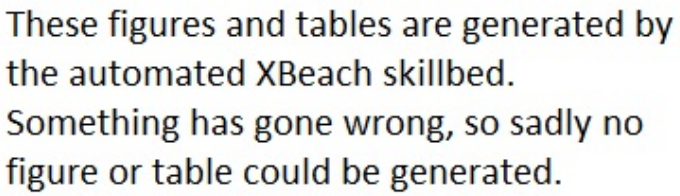


*Figure 5.3: Morphological response*

## 5.2 1976 storm surge

This test studies the impact of the 1976 storm surge on the Dutch coast at Holland. The surge during the 1976 storm was the highest since the 1953 storm. In the night between January 2nd and 3rd wind speeds reached a maximum near the Dutch coast. In the central and eastern parts of the North Sea the wind speed reached 51 m/s from the Northwest. The strongest gale on the Dutch mainland was recorded at Vlissingen: southwestern wind with a speed of 26 m/s. This caused a significant storm surge with a maximum water level in the afternoon of January 3rd (Van der Werf et al., 2011).

Between October 1975 (pre-storm) and February (post-storm) 1976 30 cross-shore profile measurements were performed at eight locations (among others) along the North-Holland coast. The observed profiles generally extend from the low water line to above the dune foot (+3 m NAP). We have extended these with the latest JARKUS data (yearly profile measurement from approximately -8 m NAP to the first dune row), measured in spring 1975. 1D XBeach models were setup for these 30 transects, of which 3 are used in this test.

We base the XBeach model settings on an extensive sensitivity analysis and on recent XBeach studies (Van der Werf and Van Santen, 2010). Furthermore, we take a morphological acceleration factor of 1, set the offshore boundary at a depth of 20 m, and use measured instead of computed water levels as input.

As an example, Figure 5.4 shows the initial cross-shore profile with the pre-storm measurement, the post-storm measurement and the final profile predicted by XBeach for one of the 30 transects. **??** shows the Brier Skill Score of all computed transects.

*Figure 5.4*

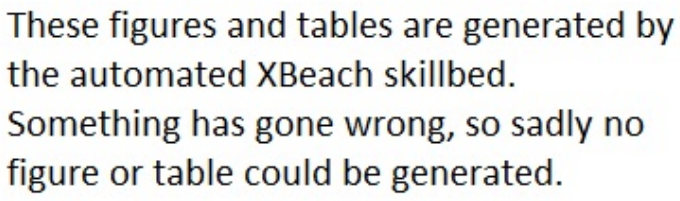


*Figure 5.5: Overview of Brier Skill Scores*

## 5.3 Erosion and overwash of Asseteague Island

This test concerns the morphodynamic response of sandy dunes to extreme storm impacts at Assateague Island, Maryland, USA, which was analyzed before by Jimenez et al. (2006). Two consecutive North Easters attacked the barrier island during late January and early February, 1998. The bathymetry was measured using LIDAR in September 1997 and again February 9th and 10th, 1998 after the two storms had subsided.

Three types of dunes were identified by Jimenez et al. (2006), shown in Figure 5.6. Profile A (upper left panel) is initially characterized by a steep faced dune, where the maximum run-up exceeded the dune crest height and the mildly sloped back of the dune. The morphological response is characterised by profile lowering, decrease of the beach face slope and landward barrier displacement, while retaining barrier width.

Profile type B is a double-peaked dune profile and has two different shapes. Profile B1 (upper right panel) is initially characterized by a primary and secondary dune, both of which are lower than the maximum run-up height and which are separated by a valley. Profile B2 (bottom left panel) initially has two peaks of which the seaward one is lower. The backside of the barrier of either type is therefore either characterized by a secondary dune line (profile B1) or a taller crest of the dune (profile B2) which prevents the eroded sand from being transported to the backside of the dune. The main morphological response for these profile types is a decrease of the beach face slope, outer shoreline retreat and narrowing of the barrier.

The height of the dune crest of profile C (lower right panel) exceeds the maximum run-up height and so little overwash is observed. The morphological response of this type of profile is crest lowering due to slumping, decrease of the beach face slope and retreat of the outer shoreline. The width of the barrier is seen to decrease.

The storm impact of the two North Easters on Assateague Island were modelled with XBeach for the four profiles described by Jimenez et al. (2006). The profiles were extended with a shallow foreshore and a 1:100 slope in seaward direction till a water depth of 9 m below NAVD88. As XBeach has not been shown to accurately simulate morphological change during very long storm durations, the simulations were run for a total of 20 hours. The measured wave and surge conditions were parameterized for each storm by a constant surge level and a constant wave spectrum (Pierson-Moskowitz) (see Table 5.1). This approach assumes that two 72 hour storms with varying surge and wave conditions can be approximated by two 10 hour simulations with constant maximum surge and wave conditions following a similar approach as Vellinga (1986). This approach also facilitates further sensitivity studies into the effect of varying hydraulic forcing conditions. The calculation grid size varies from 18 m at the offshore boundary to 2 m on the islands. A morphological acceleration factor of 5 is applied. The final simulated bed profiles are shown in Figure 5.6.

*Table 5.1: Hydrodynamic boundary conditions XBeach simulations*

These figures and tables are generated by
the automated XBeach skillbed.
Something has gone wrong, so sadly no
figure or table could be generated.

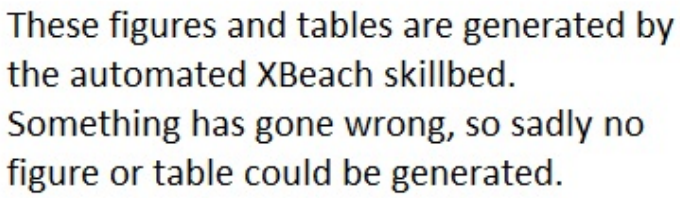


*Figure 5.6: Pre-storm profiles (black dotted line), measured post-storm profiles (black solid line) and modelled post-storm profiles (red solid line). Upper left panel: profile A. Upper right panel: profile B1. Lower left panel: profile B2. Lower right panel: profile C. The seaward side is on the left in all panels. Note that the measured post-storm profiles contain only the sea surface and emerged topography and no submerged topography.*

## 5.4 Breach growth at Zwin

This test is absed on the Zwin breach growth experiment, as reported by Visser (1998). In the mouth of the Zwin, a tidal inlet located at the border between the Netherlands and Belgium, an artificial dam was constructed with a crest height of 3.3 m +N.A.P. (Dutch datum, approx. MSL), crest width 8 m, inner slope 1:3 outer slope 1:1.6 and length 250 m. An initial depression of 0.8 m was made in the middle of the dam having a width of 1 m and a side slope of 1:1.6 to ensure that the breach initiated at this location. The level of the surrounding sea bed was about 0.7 m + N.A.P. The mean tidal prism of the Zwin is about 350,000 m3. The polder area $A_p$ as a function of the water level behind the dam is given by:

$$\begin{aligned} A_p &= 170.000m \cdot z_s - 100.000m^2 \quad , \quad 0.6m < zs < 2.3m + NAP \\ A_p &= 2.100.000m \cdot z_s - 4.540.000m^2 \quad , \quad zs \geq 2.3m + NAP \end{aligned}$$

At t = 0, about 10 minutes prior to high water, the water level at the seaside was 2.72m+NAP. At t = 10 minutes a water level of 2.75m+NAP. was reached. For the remainder of the test, which had a total duration of 1 hour, the water level marginally decreased. After 1 hour the breach growth became nil, as the water level of the polder area behind the breached equaled the sea level. The wave height near the dam was negligible during the experiment. The wind speed was about 2 m/s.

Until t = 6.5 minutes the breach depth grew whereas the breach width remained constant. At t = 6.5 minutes the original dike structure had nearly completely disappeared over the initial depression width of 1 m. Near t = 6.5 minutes the onset of lateral breach growth was observed. The scour hole developed further down to a depth of -1.6m+NAP. (4.9 m below the original dam crest level). The rate of lateral breach growth was about 2 cm/s. After approximately 40 minutes the process slowed down considerably and after approximately 1 hour the water levels at both sides were equal.

A schematized representation of the Zwin test was created in XBeach, with at the sea side a uniform bed level at 0.7m+NAP, and inside the basin a prismatic profile with the deepest point at 0.7m+NAP and sloping sides, such that the polder area as a function of the water level was in accordance with the equations above. The grid is non-equidistant with grid sizes gradually varying from 0.5 m near the breach to approx. 50 m far away from it. The median grain diameter $D_{50}$ of the bed material was set to 0.3 mm in accordance with the prototype test conditions for the artificial dam. The applied critical slopes for avalanching are the same as in other tests and standard settings were applied for the transport formulations. Waves were negligible in the test and were set to zero. The model was run with a CFL of 0.5 and remained smooth and stable despite the steep slopes and supercritical flows.

In Figure 5.7 a sequence of 3D images is shown depicting the various stages in the breaching process: the initial overflowing, the cutting back of the breach, the deepening and finally the widening of the breach.

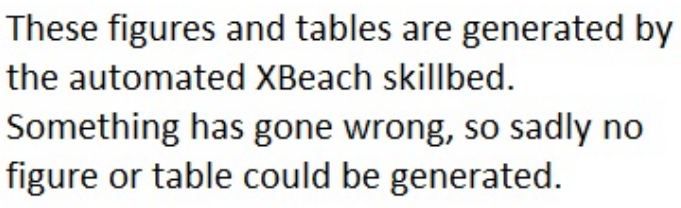


*Figure 5.7: Growth of breach width*

In Figure 5.8 a comparison is given between measured and simulated water levels, flow velocities and development of the breach width in time. Observation point MS2 is 30 m upstream of the centre point of the breach and MS4 is 30 m downstream of it. In MS4 there was some ambiguity in the measured initial water level, which explains the initial discrepancy between measurements and simulations.

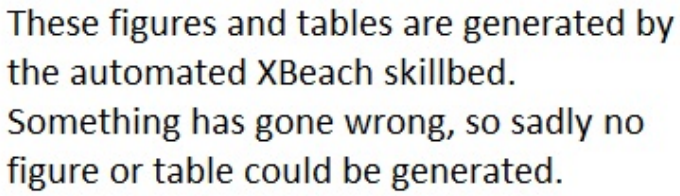


*Figure 5.8: Breach width related to water level and flow velocities*

## 5.5 MICORE field experiments

Within the European Community's Seventh Framework Programme, the MICORE project facilitated the validation of XBeach for 9 European coastal sites and compared the XBeach results to results obtained from models locally used (Deltares, 2011).

The validation of XBeach started off with a measurement campaign at each of the 9 sites. During the measurements, bathymetric and hydrodynamic data is collected, which is subsequently used as input for XBeach and the other models. The following subsections describe the results for 6 of the 9 field sites.

### 5.5.1 Lido di Dante, Italy

The study site is the Lido di Dante-Lido di Classe area, an 8 km stretch of sandy beaches along the Emilia-Romagna coastline in northern Italy on the Adriatic Sea. The site is a mixture of urbanised (approximately 40% of the total area) and relatively pristine (approximately 60%) coastal environments. The seaside towns of Lido di Dante and Lido di Classe are located at the site's northern and southern boundaries respectively. In these regions the beaches are protected by offshore breakwaters and groins and backed by moderate coastal development in the form of beach huts, holiday accommodation and paved roads. Between these two towns is a natural park consisting of natural vegetated dunes and no coastal protection. Three river mouths are located at the site: one at Lido di Dante (Fiumi Uniti); one at Lido di Classe (Fiume Savio); and one in the centre of the natural park (Torrente Bevano).

The submerged beach is generally composed of fine sand, while the beachface is made up of fine to medium sands (D50 = 0.03 mm). The intertidal beach slope varies significantly along the 8 km's of coastline, from mild (2.5%) to steep (14%). Steep values are representative of areas adjacent to coastal defence structures (i.e. groins) while the area inside the natural park is characterised by lower gradients. The mean submerged beach slope is 3%. According to the morphodynamic classification of Wright and Short (1984), the beaches are considered as having intermediate beach states. Low tide terraces are often observed both in the protected

and natural areas. Submerged longshore bars meanwhile are only present in the areas outside of the offshore structures.

The wave climate of this region is generally small, with 91% of significant wave heights below 1.25 m. The prevalent wave direction is from the east, while the most intense storms are from the ENE (known as the "Bora wind"). The Bora wind is a strong, cold, gusty wind that blows intermittently but mainly during the winter months. It not only has a strong influence on the wave climate of this region, but of the general circulation patterns of the entire Adriatic Sea. South-easterly waves meanwhile are much less significant, since SE winds are sheltered to some degree by the Conero Headland approximately 120 km south of the site.

In regards to water level variations, the area is microtidal with a mean neap tidal range of 30-40 cm and a mean spring tidal range of 80-90 cm. The tidal signal has both diurnal and semidiurnal components. Tidal anomalies of up to double the maximum tidal elevation can occur as a result of surge. This is particularly the case during SE wind conditions, where, considering the SE-NE orientation of the Adriatic Sea, there is the greatest fetch for wind-driven surge.

Within the 2008-2010 MICORE monitoring period, three storms were selected for calibration of the off-the-shelf and XBeach models. Each storm has distinct properties that encompass the range of storm conditions typical for the Emilia-Romagna region. Here the modelling is restricted to profile MN15 for the 1-3 December 2008 storm.

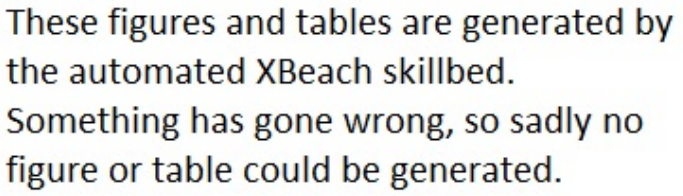


*Figure 5.9*

### 5.5.2 Praia de Faro, Portugal

The study area is Ancao Peninsula constituting the westernmost barrier of the Ria Formosa barrier island system. It is a NW-SE oriented sandy barrier that is attached to mainland by its western terminus.

The area is mesotidal, with an average tidal range of about 2 m that can reach up to 3.5 m during spring tides. Analysis of two years of records from a tidal gauge on the Algarve Coast showed a maximum observed storm surge level of +0.75 m (Gama et al., 1994). The return period of a sea level 2.23 m above Mean Sea Level (MSL) is 10 years (Gama et al., 1994).

The offshore wave climate is dominated by west-southwest waves (71% of occurrences). SE waves that consist of short period waves generated by regional winds (locally called 'Levante') are also frequent (about 23%). Wave energy is moderate with an average annual significant offshore wave height of 1.0 m and average peak period of 8.2 s (Costa et al., 2001).

Storm events in the region are considered when the significant offshore wave height exceeds 3 m (Pessanha and Pires, 1981) and typically correspond to less than 1% of the offshore wave climate (Costa et al., 2001). A 5.0 m significant wave height for a SE storm has a return period of 50 years, whilst a 5.7 m SW storm is expected every 5 years (Pires, 1998). Due to it's northwest-southeast orientation it is directly exposed to west-southwesterly waves, and is relatively protected from SE waves.

Several storm events have been recorded during the MICORE campaign among which the two most important are discussed in the MICORE report. Here a group of several individual WSW storms is simulated that took place at Faro beach from 18/12/2009 until 5/1/2010. The significant wave height reached 4 m and the peak period up to 20 sec, while given the long duration intense wave conditions coincided with both spring and neap tides. The event had a significant impact on the coast, as overtopping and dune erosion occurred at several sections.

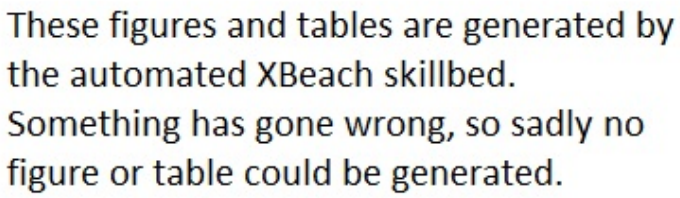


*Figure 5.10*

### 5.5.3 Cadiz Urban Beach, Spain

The field site is located around Cadiz town, in south-western Spain, facing the Atlantic Ocean. It is constituted by two different beaches extending along 10 km, providing the opportunity for studying the effects of storms on different types of coastal environments.

The study area is a mesotidal coast with a mean tidal range of 3.2 m and 1.1 m during springs and neaps tides, respectively. Dominant winds blow from ESE (19.6% of annual occurrence) and WNW (12.8%), which together with coastline orientation makes sea and swell waves approach generally from the third and fourth quadrants. According to this, prevailing longshore drift is directed south-eastwards. Significant wave height is usually lower than 1 m, with waves over 4 m high being uncommon and occurring only during the most important storms, which usually take place between November and March and approach from the third

quadrant. In fact, waves greater than 1.5 m are considered storm waves, so the area can be classified as a low-energy one.

The storm event that was selected is a moderate storm event with a return period of about 1 year. The maximum significant wave (Hs) height during the peak of the event was 3.7m with a spectral period (Tp) of 8.7sec. The total duration of the storm was 46 hours (light grey shaded area). The tidal conditions over that period were from springs to neaps with an average tidal range of 2.27m.

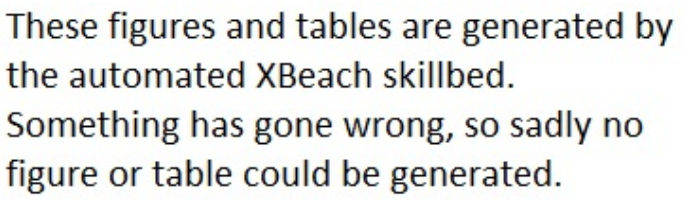


*Figure 5.11*

### 5.5.4 Dziwnow Spit, Poland

The Polish study site is the 14 km long Dziwnow Spit of barrier type built of Holocene deposits (mainly sands) with dunes 3.5 to 10 meters high. Behind the spit there are relatively wide lowlands of glacial or glaciofluvial origin, in most cases filled with peat. Their surface is 1 to 3 m above sea level. In the lowlands alos the Kaminski Lagoon is found with a rather small depth (maximum 2-3 m). At the middle of the spit there is a connection between the lagoon and sea (Dziwna). The mean beach width calculated for the pilot area is 33 m.

The average tide range in the Baltic is very small and is less then 10 cm. This is due to the small area of the Baltic, its geographical situation and the presence of the Danish Straits, which prevent propagation of North Sea tides into the Baltic. Thus, surface waves (wind waves and swell) are the most important factor of the Baltic coastal zone hydrodynamics. The wave climate in Poland is highly diversified because of the wealth of fetches and wind speeds occurring throughout the year.

Since 1 June 2008, (from the beginning of observations taken within MICORE project) 1 extreme storm (12.10.2009) was noticed which caused significant morphological changes at the shore. The storm return period was about 4 years and was simulated with the XBeach model.

The storm occurred on 12.10.2009 and lasted for almost 4 days (93hours). The highest sea level observed on tide gauge located in the Dziwna (Dziwnow Port Authority area) was 0,76 m. above mean sea level. The maximum significant wave height (Hs) reached 3.2 m and teh

maximum peak period (Tp) was 11.17 sec.

The XBeach model was run for profile 386 in 1D mode. The profile was interpolated to a cross-shore varying grid with a minimum cell size of 3 m. Offshore wave data timeseries from the WAM model were inputted to XBeach using a Jonswap spectrum and setting instat=41. Wave direction values were changed to 270 degrees, which means that incoming waves are shore normal. Surge input data were taken as the hourly mean sea level.

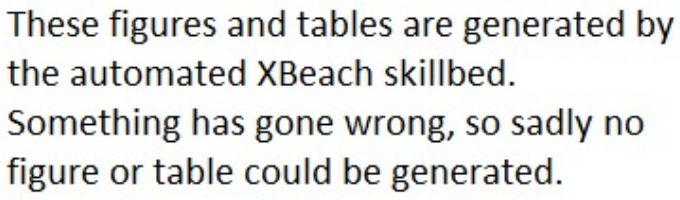


*Figure 5.12*

### 5.5.5 Kamchia Shkorpilovtsi Beach, Bulgaria

The study area, called Kamchia-Shkorpilovtsi, is situated in the western Black Sea, and spreads from cape Paletsa to cape Cherni Nos (Figure 9.1), located 25 and 40 km to the south of Varna city, respectively. It comprises the longest and the largest sandy beach along the Bulgarian Black Sea coast, with well-developed dunes and the two rivers' mouths, these of the Kamchia River and the Fundakliiska River. In the middle of the site, near the mouth of the Fundakliiska River a scientific pier is built perpendicularly to the shoreline, reaching 4.5 m water depth. The beach is formed as a result of accumulation of erosive and fluvial sediments. The main morphological feature of the study area is its rectilinear shoreline with almost parallel isobaths. The bottom slope is covered with sands of different size. In its upper part down to 2.5 m depth, over 95% of bottom sediments consist of coarse and medium sand fractions. As the depth grows, the content of these fractions decreases and at 8-10 m over 90% of the sediment grain size is less than 0.25 mm.

The beach is open to waves of the eastern half. In the case of severe storms the wind speed magnitude can reach 35-40 m/s and 9 m height of maximum significance wave at depths of about 1000 m. The large seasonal variability is one of the most marked features of the wave climate. The winter storms are much more frequent than the summer ones. In the western Black Sea the most frequent are the winds from northeast and east, which trigger the most severe storms.

In the beginning of March a short but very intense storm occurred in the western Black sea. This event was distinguished with all features of the severe storms known from the historical overview well defined phases growth took place on 08.03, peak 09.03 and decay 09.03 - 10.03.

Wind and wave direction were quite stable turning from ESE to ENE. Maximum SWH reached almost 4.20 m.

Model results for this storm are shown in Figure 5.13.

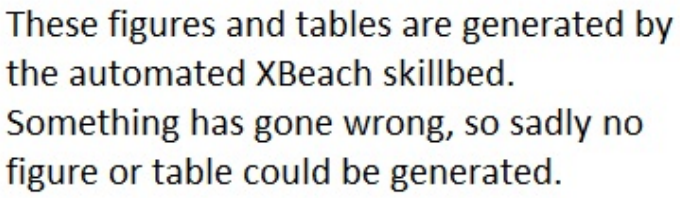


*Figure 5.13*

# Chapter 6

# Comparisons with other models

In this chapter, XBeach is compared to results obtained from other models. The comparisons are currently focussed on the DUROS+ and D++ (Vellinga, 1986; Delft Hydraulics, 2006; Deltares, 2010) models that are used for the assessment of dunes along the Dutch coast. Comparisons with other models like DurosTA (Steetzel, 1993) are made throughout the report and are not discussed specifically in this chapter at the moment.

## 6.1 Field applications

In this section, DUROS+ (Vellinga, 1986; Delft Hydraulics, 2006) and D++ are (Deltares, 2010) compared with XBeach based on field applications. Comparisons are made based on erosion volumes and retreat distances, since these are the main parameters of interest in dune safety assessment.

### 6.1.1 Retreat distances JARKUS

In this test, retreat distances obtained from DUROS+ and XBeach using a selection of JARKUS profiles characteristic for the Dutch coast are compared (Den Heijer et al., 2011). The comparison is presented in Figure 6.1. The retreat distance is defined as the horizontal distance between the NAP+5m contour and the erosion point. The erosion point is defined as the first diversion point between the pre-storm and post-storm profile, when going from the land side in seaward direction. Diversion is considered as a vertical difference of more than 5cm.

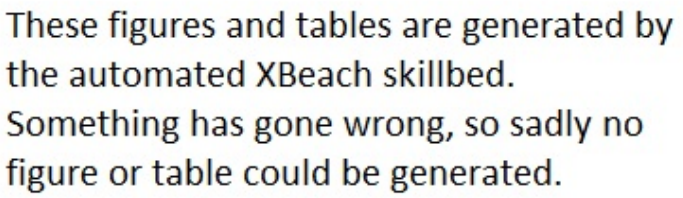


*Figure 6.1: Scatter plot of retreat distances obtained from XBeach and DUROS+ (blue circle) and XBeach and D++ (green cross).*

# Chapter 7

# Specific functionalities

In the previous chapters, the core functionalities are discussed: hydro- and morphodynamics on different scales. However, XBeach is equipped with a variety of additional functionalities that facilitate more complex computations. One example already discussed is hard elements in the profiles. This chapter discusses a variety of other functionalities, like discharges, drifters and multiple sediment fractions.

## 7.1 River outflow

The river outflow case is meant to test XBeach for the combined effects of a river outflow and a steady wave-driven longshore current on the sediment transport and the morphological evolution. Though purely hypothetical, this case contains many salient features of real-life applications, such as longshore currents through open side-boundaries and exchange of water and sand through a gap in a closed boundary. Thus, the formulation of open boundary conditions is also tested here.

The initial topography consists of a plane beach (slope 1:50), which is interrupted by a 75 m wide river mouth with a water outflow of 150 $m^3/s$. The bottom contours are straight and parallel to the shoreline, except for a shallow submerged channel in line with the river.

The computational grid is rectangular, with 56 nodes in the x-direction (cross-shore) and 111 nodes in the y-direction (longshore), with a uniform grid spacing of 15 m. The waves are irregular and long-crested, with a root-mean-square height of 2m at a water depth of 13.5m. The direction of wave incidence is 30 degrees with respect to the shore-normal. The peak wave period is 8s. The bed material is uniform sand of 250, with a settling velocity of 0.031m/s.

In this figure the bathymetry is shown after approxiately 4 days; arrows indicate the sediment transport vectors. plotted for every cross-shore cell and every third longshore cell. When functioning correctly, we see a channel that has turned towards the north and striaght contour lines downstream of the channel.

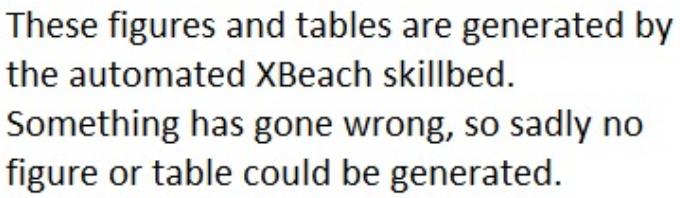


*Figure 7.1: Final bathymetry*

## 7.2 Drifters

This purely hypothetical test combines three specific functionalities of XBeach: curvilinear grids, discharges and drifters. The model is basicly an odd-shaped bathtub with a single discharge location at the left boundary. The bathtub is filled by the discharged water, indicated by the increasing water levels (colored background). The bathtub is approximately 70m x 70m. Considering that, the discharge of $50m^3/s$ is rather large. Every 10 seconds, two drifters are released just before the discharge opening. One of the two drifters is released at the upper boundary of the opening, the other at the lower boundary. The entire path a single drifter has followed at a certain moment in time is plotted in Figure 7.2. Two large eddies driven by the large discharge are revealed by these paths.

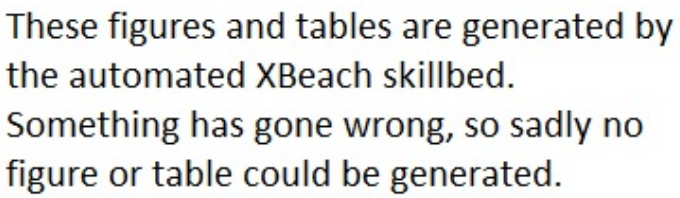


*Figure 7.2: Drifter paths after 50, 100, 150 and 450 seconds*

## 7.3 Multiple sediment fractions

The purpose of this simulation is to ensure the multiple sediment fractions model in XBeach performs as expected. In this test, the Deltaflume 2006 T01 test is recreated with two types of sand with different colours, red and blue. The sand is initially placed in a zebra-stripe pattern in the profile. The properties of both types of sand such as the grain size and mobility are the same as the sand used in the Deltaflume experiment. For the test to be successful, the following conditions should be met:

1. The simulated final profile should be the same as the final profile in the original Deltaflume 2006 T01 test.
2. The two sediment types should mix and form layers over each other (yellow).

The figures Figure 7.3 and Figure 7.4 show the initial and final distribution of red and blue sediment in the profile near the dune face. The red and blue lines in the same figure show the sediment concentration of each sediment type in the water column. If the simulation is successful, the red and blue sediment will be well mixed on the foreshore and fresh blue sediment will be deposited over the red sediment at the dune foot as the dune face retreats. The concentration of blue sediment in the water column should be higher than the concentration of red sediment in the water in areas where only blue sediment is available in the top layer of the bed.

The red lines in Figure 7.5 show the predicted dune face retreat and bed level change in the XBeach multiple-sediment model. The black lines in the same figure are the corresponding measured profiles. If the simulation has been successful, the red and black lines will align reasonably well. The results of this simulation should be compared to the Deltaflume 2006 T01 test described earlier in this report.

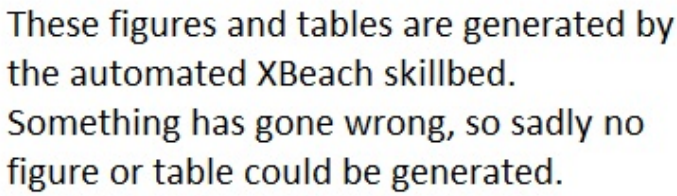


*Figure 7.3: Initial bathymetry and sediment distribution*

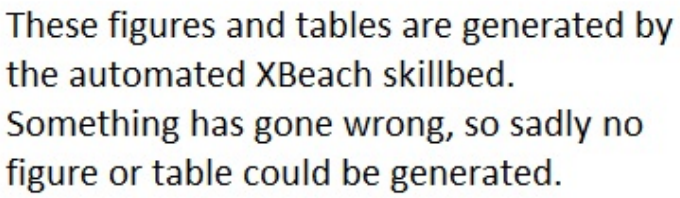


*Figure 7.4: Final bathymetry and sediment distribution*

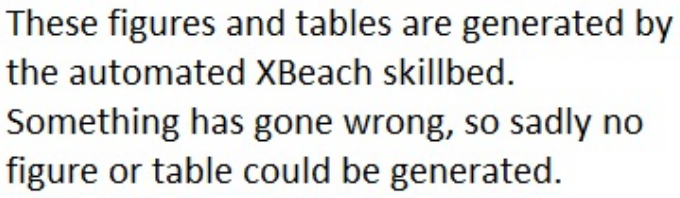


*Figure 7.5: Profile development*

## 7.4 Curvilinear

In this test a curvi-linear grid is applied to simulate waves and hyrdodynamics around a virtual island. The island is circular with a linear sloping profile. The lower half of the offshore boundary generates bichromatic waves that partly refract towards the island, but also passes the island. The waves passing the island leave the model through the upper half of the offshore boundary. Reflections at the offshore boundary are minimal due to the 2D weakly-reflective boundary condition used (Van Dongeren and Svendsen, 1997).

Figure 7.6 shows the RMS wave height (color) and the flow velocity field (arrows) around the island in the last time step. Figure 7.7 shows the same parameters, but in this case the overall mean values are presented.

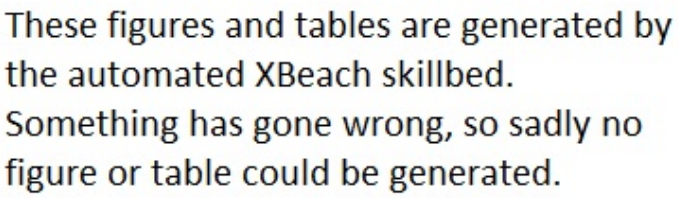


*Figure 7.6: Snapshot of the RMS wave height and the flow velocity field in the last time step*

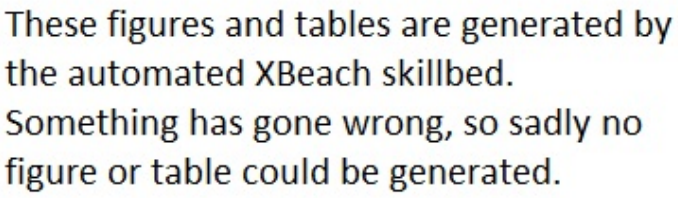


*Figure 7.7: Mean values of the RMS wave height and the flow velocity field*

# Chapter 8

# References

Abdelrahman, S. M. and Thornton, E. B. (1987). Changes in the short wave amplitude and wavenumber due to presence of infragravity waves. In *Proceedings Speciality Conference on Coastal Hydrodynamics*, pages 458–478. 42

Arcilla, A. S., Roelvink, J. A., O'Connor, B. A., Reniers, A., and Jimenez, J. A. (1994). The delta flume '93 experiment. In *Coastal Dynamics*, pages 488–502. 37, 39

Bakkenes, H. J. (2002). Observation and seperation of bound and free low-frequency waves in the nearshore zone. Master's thesis, Delft University of Technology. 12

Birkemeier, W. A., Donoghue, C., Long, C. E., Hathaway, K. K., and Baron, C. F. (1997). 1990 delilah nearshore experiment: Summary report. Technical Report CHL-97-4-24, U.S. Army Corps of Engineers. Field Research Facility. 13

Boers, M. (1996). Simulation of a surf zone with barred beach, part 1: Wave heights and wave breaking. Communications on Hydraulic and Geotechnical Engineering 69-5, Delft University of Technology. 116 p. 12

Carrier, G. F. and Greenspan, H. P. (1958). Water waves of finite amplitude on a sloping beach. *Journal of Fluid Mechanics*, 4:97–109. 8, 9

Costa, M., Silva, R., and Vitorino, J. (2001). Contribuio para o estudo do clima de agitao martima na costa portuguesa. In *2as Jornadas Portuguesas de Engenharia Costeira e Porturia*, page 20p, Sines. in Portuguese. 69

Damgaard, J., Dodd, N., Hall, L., and Chesher, R. (2002). Morphodynamic modelling of rip channel growth. *Coastal Engineering*, 45:199–221. 2

Delft Hydraulics (2006). Dune erosion – product 2: Large-scale model tests and dune erosion prediction method. Report H4357, Delft Hydraulics. 73

Deltares (2010). Ontwikkeling detailtoets duinen 2011. Interim report 1202124-003, Deltares. in Dutch. 73

Deltares (2011). Validation of dune impact models using european field data. Report 1002266, Deltares. 67

Den Heijer, C., Walstra, D. J. R., Van Thiel de Vries, J. S. M., Huisman, B. J. A., Hoonhout, B. M., Diermanse, F. L. M., and Van Gelder, P. H. A. J. M. (2011). Importance of dune erosion influencing processes. *Journal of Coastal Research*, SI 64(1):283–287. ISSN 0749-0208. 73

Dongeren, A. V., Lowe, R., Pomeroy, A., Trang, D. M., Roelvink, D., Symonds, G., and Ranasinghe, R. (2013). Numerical modeling of low-frequency wave dynamics over a fringing coral reef. *Coastal Engineering*, 73(0):178 – 190. 16, 17

Erikson, L., Larson, M., and Hanson, H. (2005). Prediction of swash motion and run-up including the effects of swash interaction. *Coastal Engineering*, 52:285–302. 2

Feddersen, F., Guza, R. T., Elgar, S., and Herbers, T. C. (2000). Velocity moments in alongshore bottom shear stress parameterizations. *Journal of Geophysical Research*, 105:8673–8688. 2

Gama, C., Dias, J. A., Ferreira, O., and Taborda, R. (1994). Analysis of storm surge in portugal, between june 1986 and may 1988. In *Proceedings Second International Symposium on Coastal Zone Research - Management and Planning*, pages 381–387, Lisbon. EUROCOAST. 68

Huntley, D. A., Guza, R. T., and Thornton, E. B. (1981). Field observations of surf beats, 1, progressive edge waves. *Journal of Geophysical Research*, 86:6451–6466. 2

Jimenez, J. A., Sallenger, A. H., and Fauver, L. (2006). Sediment transport and barrier island changes during massive overwash events. In *30th International Conference on Coastal Engineering*, San Diego, California, USA. ASCE. 63, 64

Larson, M., Erikson, L., and Hanson, H. (2004). An analytical model to predict dune erosion due to wave impact. *Coastal Engineering*, 51(8–9):675–696. 1, 3

Leatherman, S. P., Williams, A. T., and Fisher, J. S. (1977). Overwash sedimentation associated with a large-scale northeaster. *Marine Geology*, 24:109–121. 3

List, J. H. (1992). A model for two-dimensional surfbeat. *Journal of Geophysical Research*, 97:5623–5635. 2

Murphy, A. H. and Epstein, E. S. (1989). Skill scores and correlation coefficients in model verification. *Monthly Whether Review*, 117:572–581. v, 89, 91, 92

Nairn, R. B., Roelvink, J. A., and Southgate, H. N. (1990). Transition zone width and implications for modelling surfzone hydrodynamics. In Edge, B. L., editor, *22th International Conference on Coastal Engineering*, pages 68–81, Reston, Virginia, USA. ASCE. 2

Nishi, R. and Kraus, N. C. (1996). Mechanism and calculation of sand dune erosion of storms. In *25th International Conference on Coastal Engineering*, pages 3034–3047, Orlando, Florida, USA. ASCE. 1

Overton, M. F. and Fisher, J. S. (1988). Laboratory investigation of dune erosion. *Journal of Waterway, Port, Coastal and Ocean Engineering*, 114(3):367–373. 1

Özkan-Haller, H. T. and Kirby, J. T. (1997). A fourier-chebyshev collocation method for the shallow water equations including shoreline runup. *Applied Ocean Research*, 19:21–34. 9, 11

Phillips, O. M. (1977). *The Dynamics of the Upper Ocean*. Cambridge University Press, New York, 2nd edition. 2

Pires, H. O. (1998). Project india, preliminary report on wave climate at faro. Technical report, Instituto de Meteorologia, IST, Lisbon. 69

Pomeroy, A., Lowe, R., Symonds, G., Dongeren, A. V., and Moore, C. (2012). The dynamics of infragravity wave transformation over a fringing reef. *Journal of Geophysical Research*, 117(C11022):1 – 17. 16

Raubenheimer, B. and Guza, R. T. (1996). Observations and predictions of run-up. *Journal of Geophysical Research*, 101(C10):25,575–25,587. 2

Reniers, A. J. H. M., MacMahan, J., Thornton, E. B., and Stanton, T. P. (2006). Modelling infragravity motions on a rip-channel beach. *Coastal Engineering*, 53:209–222. 2

Reniers, A. J. H. M., Roelvink, J. A., and Thornton, E. B. (2004a). Morphodynamic modelling of an embayed beach under wave group forcing. *Journal of Geophysical Research*, 109(C01030). 2

Reniers, A. J. H. M., Thomas, E. B., Stanton, T. P., and Roelvink, J. A. (2004b). Vertical flow structure during sandy duck: observations and modeling. *Coastal Engineering*, 51(3):237–260. 2

Roelvink, J. A. (1993a). Dissipation in random wave groups incident on a beach. *Coastal Engineering*, 19:127–150. 2

Roelvink, J. A. (1993b). *Surf beat and its effect on cross-shore profiles*. PhD thesis, Delft University of Technology. 2

Roelvink, J. A., Reniers, A. J. H. M., Van Dongeren, A. R., Van Thiel de Vries, J. S. M., McCall, R. T., and Lescinski, J. M. (2009). Modelling storm impacts on beaches, dunes and barrier islands. *Coastal Engineering*, 56(11-12):1133–1152. 1

Roelvink, J. A. and Stive, M. J. F. (1989). Bar-generating cross-shore flow mechanisms on a beach. *Journal of Geophysical Research*, 94(C4):4785–4800. 42

Roelvink, J. A., Van Kessel, T., Alfageme, S., and Canizares, R. (2003). Modelling of barrier island response to storms. In *Coastal Sediments '03*, Clearwater, Florida, USA. 3

Ruessink, B. G., Miles, J. R., Feddersen, F., Guza, R. T., and Elgar, S. (2001). Modeling the alongshore current on barred beaches. *Journal of Geophysical Research*, 106:22,451–22,462. 2

Sallenger, A. H. (2000). Storm impact scale for barrier islands. *Journal of Coastal Research*, 16(3):860–895. 2

Schaeffer, H. A. (1994). Edge waves forced by short-wave groups. *Journal of Fluid Mechanics*, 259:125–148. 2

Soulsby, R. L. (1997). *Dynamics of Marine Sands*. Thomas Telford, London. 2

Soulsby, R. L., Hamm, L., Klopman, G., Myrhaug, D., Simons, R. R., and Thomas, G. P. (1993). Wavecurrent interaction within and outside the bottom boundary layer. *Coastal Engineering*, 21:41–69. 2

Steetzel, H. J. (1987). Systematic research on the effectiveness of dune toe revetments - large scale model investigation. Technical Report H298-I, Delft Hydraulics. 36

Steetzel, H. J. (1993). *Cross-shore transport during storm surges*. PhD thesis, Delft University of Technology. 1, 73

Stelling, G. S. and Duinmeijer, S. P. A. (2003). A staggered conservative scheme for every froude number in rapidly varied shallow water flows. *International Journal for Numerical Methods in Fluids*, 43:1329–1354. 3

Stive, M. J. F. and De Vriend, H. J. (1994). Shear stresses and mean flow in shoaling and breaking waves. In Edge, B. L., editor, *24th International Conference on Coastal Engineering*, pages 594–608, Reston, Virginia, USA. ASCE. 2

Stockdon, H. F., Holman, R. A., Howd, P. A., and Sallenger, A. H. (2006). Empirical parameterization of setup, swash, and runup. *Coastal Engineering*, 53:573–588. 2

Sutherland, J., Peet, A. H., and Soulsby, R. L. (2004). Evaluating the performance of morphological models. *Coastal Engineering*, 51(8–9):917–939. 89

Svendsen, I. A. (1984). Wave heights and set-up in a surf-zone. *Coastal Engineering*, 8:303–329. 2

Thornton, E. B., MacMahan, J., and Sallenger, A. H. (2007). Rip currents, mega-cusps, and eroding dunes. *Marine Geology*, 240(1–4):151–167. 1

Tucker, M. J. (1954). Surfbeats: sea waves of 1 to 5minutes' period. In *Proceedings of Royal Society*, number A in 202, pages 565–576, London. 2

Van de Graaff, J. (1976). Scale series dune erosion. Technical Report M1263 part I, Delft Hydraulics. in Dutch. 26, 27, 28

Van der Werf, J., Van Santen, R., Van Ormondt, M., Briere, C., and Van Dongeren, A. (2011). Operational model to simulate storm impact along the holland coast. In *Proceedings Coastal Sediments 2011*, Miami, Florida, USA. 62

Van der Werf, J. J. and Van Santen, R. (2010). Operational model to simulate storm impact along the holland coast: system development and test application. Technical report, Deltares, Alkyon and Arcadis. 63

Van Dongeren, A. R., Reniers, A. J. H. M., Battjes, J. A., and Svendsen, I. A. (2003). Numerical modeling of infragravity wave response during delilah. *Journal of Geophysical Research*, 108(C9):3288. 2, 14

Van Dongeren, A. R. and Svendsen, I. A. (1997). Absorbing-generating boundary condition for shallow water models. *Journal of Waterway, Port, Coastal and Ocean Engineering*, pages 303–313. 78

Van Gent, M. R. A., Van Thiel de Vries, J. S. M., Coeveld, E. M., De Vroeg, J. H., and Van de Graaff, J. (2008). Large-scale dune erosion tests to study the influence of wave periods. *Coastal Engineering*, 55(12). 1, 41, 42, 49, 54, 57, 58

Van Rijn, L. C., Walstra, D. J. R., Grasmeijer, B., Sutherland, J., Pan, S., and Sierra, J. P. (2003). The predictability of cross-shore bed evolution of sandy beaches at the time scale of storms and seasons using process-based profile models. *Coastal Engineering*, 47(3):295–327. ISSN 0378-3839. 91, 92

Van Thiel de Vries, J. S. M. (2009). *Dune erosion during storm surges*. PhD thesis, Delft University of Technology. 42, 44, 49

Van Thiel de Vries, J. S. M., Van Gent, M. R. A., Walstra, D. J. R., and Reniers, A. J. H. M. (2008). Analysis of dune erosion processes in large-scale flume experiments. *Coastal Engineering*, 55(12). 2, 41

Vellinga, P. (1981). Scale series dune erosion. Technical Report M1263 part II, Delft Hydraulics. in Dutch. 27, 28

Vellinga, P. (1984). Scale series dune erosion: Large scale tests in deltaflume. Technical Report M1263 part III, Delft Hydraulics. in Dutch. 29, 61

Vellinga, P. (1986). *Beach and Dune Erosion during Storm Surges*. PhD thesis, Delft University of Technology. 1, 28, 36, 61, 64, 73

Visser, P. J. (1998). *Breach growth in sand dikes*. PhD thesis, Delft University of Technology. 3, 65

Wang, P. and Horwitz, M. H. (2007). Erosional and depositional characteristics of regional overwash deposits caused by multiple hurricanes. *Sedimentology*, 54:545–564. 3

Zelt, J. A. (1986). *Tsunamis: the response of harbours with sloping boundaries to long wave excitation*. PhD thesis, W.M. Keck Laboratory of Hydraulics and Water Resources, Division of Engineering and Applied Science, California Institute of Technology. 318 p. 9, 10, 11

# Appendix A

# Release information

## A.1 Release notes

We have been working on a lot of cool stuff that still needs to be described in more detail:

- hard structures
- multiple sediment fractions
- bed load and suspended load
- output options
- wave schemes
- non-hydrostatic model
- wave shap parameterization
- drifters
- river outflow
- boundary condition stuff
- ...

## A.2 Change log

# Appendix B

# Model Performance Statistics

## B.1 Introduction

In this Appendix the theory behind the Model Performance Statistics (MPS) used in the XBeach skillbed is explained. The MPS are used to quantify the performance of model results based on a comparison with measurement data. Different MPS parameters are used as each parameter has its own characteristics.

First an overview is given of the MPS parameters used in the XBeach skillbed, summarized in table form including some basic characteristics. Consequently, each MPS parameters listed in the overview table is further explained in separate sections.

## B.2 MPS parameters

An overview of the MPS parameters used in the XBeach skillbed is given in Table B.1.

*Table B.1: MPS parameters*

| Parameter | Description | Ranges |
|---|---|---|
| ME & STD | Mean Error & Standard Deviation | 0: perfect prediction |
| R | Correlation coefficient (range: [0 1]) | 1: perfect correlation |
| Rel. bias | Systematic error relative to the mean | low value: good performance |
| Sci | Scatter Index | low values: performance |
| BSS | Brier Skill Score (Sutherland et al., 2004) | see below |
| BSS | Brier Skill Score (Murphy and Epstein, 1989) | see below |

Each parameter listed in the table is further explained in the following paragraphs.

## B.3 Mean Error & Standard Deviation

The Mean Error (ME) and the Standard Deviation (STD) of the error of a time series are a useful measure to quantify model performance for parameters such as wave heights or water levels. The SD is in general not so useful when applied to morphological parameters such as the bed level evolution.

$$ME = \frac{1}{N}\sum_{i=1}^{N}(f_{comp.,i} - f_{meas.,i}) \tag{B.1}$$

$$STD = \sqrt{\frac{1}{N-1}\sum_{i=2}^{N}(f_{comp.,i} - f_{meas.,i} - ME)^2} \tag{B.2}$$

## B.4 Correlation coefficient

The Correlation Coefficient R is a measure quantifying the correlation of the measurements and simulation results, but does not indicate significance because the distributions of the series are not taken into account.

## B.5 Relative Bias

The Relative Bias (Rel. Bias) is the systematic error relative to the mean. Relative low values of the mean can cause high vales of the Rel. Bias.

$$Rel.Bias = \frac{\sum_{i=1}^{N}(f_{comp.,i} - f_{meas.,i})}{\sum_{i=1}^{N}\bar{f}_{meas.}} \tag{B.3}$$

## B.6 Scatter Index

The Scatter index (Sci) is the standard deviation relative to the mean value of the measured signal. Relative low values of the mean can cause high vales of the Sci.

$$Sci = \frac{\sqrt{\frac{1}{N-1}\sum_{i=2}^{N}(f_{comp.,i} - f_{meas.,i} - ME)^2}}{\bar{f}_{meas.}} \tag{B.4}$$

## B.7 Brier Skill Score

The Brier Skill Score (BSS) calculates the performance of the performance relative to a baseline prediction. The BSS calculates the mean square difference between the prediction

and observation with the mean square difference between baseline prediction and observation.

$$BSS = 1 - \frac{\frac{1}{N}\sum_{i=1}^{N}(z_{b,c} - z_{b,m})^2}{\frac{1}{N}\sum_{i=1}^{N}(z_{b,0} - z_{b,m})^2} \tag{B.5}$$

where $z_{b,c}$ is the computed bottom, $z_{b,m}$ is the measured bottom and $z_{b,0}$ is the initial bottom (variables taken at each cross-shore coordinate i).

Perfect agreement gives a Brier score of 1, whereas modelling the baseline condition gives a score of 0. If the model prediction is further away from the final measured condition than the baseline prediction, the skill score is negative. Van Rijn et al. (2003) proposed a classification for the Brier Skill Score as shown in Table B.2.

The BSS is very suitable for the prediction of bed evolution. The baseline prediction for morphodynamic modelling will usually be that the initial bed remains unaltered. In other words, the initial bathymetry is used as the baseline prediction for the final bathymetry. A limitation of the BSS is that it cannot account for the migration direction of a bar; it just evaluates whether the computed bed level (at time t) is closer to the measured bed level (at time t) than the initial bed level. If the computed bar migration is in the wrong direction, but relatively small; this may result in a higher BSS compared to the situation with bar migration in the right direction, but much too large. The BSS will even be negative, if the bed profile in the latter situation is further away from the measured profile than the initial profile. The limitation shown here is that position and amplitude errors are included in the BSS. Distinguishing position errors from amplitude errors, requires a visual inspection of measured and modelled profiles or the calculation of further statistics (Murphy and Epstein, 1989). The BSS can be extremely sensitive to small changes when the denominator is low, in common with other non-dimensional skill scores derived from the ratio of two numbers.

*Table B.2: Brier Skill Score quantification (Van Rijn et al., 2003)*

| Qualification | Brier Skill Score |
|---|---|
| Excellent | 1.0 - 0.8 |
| Good | 0.8 - 0.6 |
| Reasonable fair | 0.6 - 0.3 |
| Poor | 0.3 - 0.0 |
| Bad | <0.0 |

## B.8 Brier Skill Score (Murphy and Epstein, 1989)

Murphy and Epstein (1989) decomposed the BSS, leading to contributions due to errors in predicting the amplitude ($\alpha$), the phase ($\beta$) and the mean ($\gamma$) as presented in Table B.3. The decomposition facilitates linking performance quantifications to model processes and accordingly bringing the model performance to a higher level.

$$BSS = \frac{\alpha - \beta - \gamma + \epsilon}{1 + \epsilon} \tag{B.6}$$

$$\alpha = r^2_{Y'X'}; \beta = (r_{Y'X'} - \frac{\sigma_{Y'}}{\sigma_{X'}})^2; \gamma = (\frac{<Y'> - <X'>}{\sigma_{X'}})^2; \epsilon = \frac{<X'>^2}{\sigma_{X'}} \tag{B.7}$$

*Table B.3: Brier Skill Score decomposition factors (Murphy and Epstein, 1989)*

| Factor | Indication | Perfect modelling |
|---|---|---|
| phase error ($\alpha$) | transport locations | $\alpha = 1$ |
| amplitude error ($\beta$) | transport volumes | $\beta = 0$ |
| map mean error ($\gamma$) | - | $\gamma = 0$ |
| normalization term ($\epsilon$) | - | - |

Van Rijn et al. (2003) also proposed a classification for the decomposed Brier Skill Score as shown in Table B.4.

*Table B.4: Brier Skill Score (Murphy and Epstein, 1989) quantification (Van Rijn et al., 2003)*

| Qualification | Brier Skill Score |
|---|---|
| Excellent | 1.0 - 0.5 |
| Good | 0.5 - 0.2 |
| Reasonable fair | 0.2 - 0.1 |
| Poor | 0.1 - 0.0 |
| Bad | <0.0 |